Boulder Atmosphere Innovation Research

Boulder A.I.R. L.L.C; 2820 Lafayette Dr., Boulder, CO 80305, U.S.A.; dh.bouldair@gmail.com

January 30, 2021

To:

City of Longmont
350 Kimbark Street
Longmont, CO 80501

Attn: Dr. Jane Turner

Re: Longmont Regional Air Quality Study – Year 2020 Quarter 3 Report

Dear Dr. Turner,

Please find included with this letter the July – September (Quarter 3) 2020 report for our work on the Longmont Air Quality Study. The monitoring data and data interpretations are presented.

Thank you for providing this opportunity for air quality monitoring to Longmont citizens and the City of Longmont. We would be happy to discuss any questions that you, other City staff or Longmont citizens may have.

Sincerely,

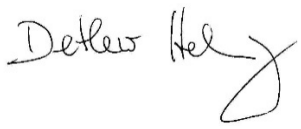

Detlev Helmig

Boulder AIR LLC

2020 Quarter 3 (July – September) Report

Longmont Air Quality Study

Executive Summary

This report summarizes the data and preliminary findings from the Longmont Air Quality Study during July through September of 2020, i.e. quarter 3 (Q3), 2020. All variables were reported in near-real time on the public *Longmont Air Quality Now* web portal. This report includes graphical analyses of all data that were acquired during Q3. In addition, data comparisons and analyses of selected events that resulted in enhanced concentrations or unusual conditions are presented. Longmont Municipal Airport (LMA) and Longmont Union Reservoir (LUR) data are compared with each other and also with concurrent observations from the Boulder Reservoir (BRZ), and the Broomfield Soaring Eagle Park (BSE) and Broomfield Livingston (BLV) monitoring sites.

There were several remarkable air quality events in Q3. From a weather perspective, an extreme cold front impacted the region in early September, causing snow and below-freezing temperatures much earlier than in most other years. The cold front, moving in from the north, brought in some remarkably clean air into the Front Range.

The late summer saw an abundance of days with high ozone. Exceedances of the ozone National Ambient Air Quality Standard (NAAQS) were observed on nine days total in Q3 at the two sites. This was also the first time since the onset of the monitoring when the NAAQS for particulates was exceeded. The 24-hour 35 $\mu g\ m^{-3}$ PM2.5 NAAQS was exceeded on a total of ten days in the LUR measurements. This significant degradation of air quality was largely caused by fire smoke plumes that were transported across the Northern Colorado Front Range. Some of these fire plumes originated in Colorado; others originated outside the state, mainly in California.

Table of Contents

1. Project Scope and Goals

No changes from Q2 report.

2. Overview of the Monitoring Program

No changes from Q2 report.

3. Air Quality Monitoring Study Updates

No changes from Q2 report.

4. Data Quality Assurance/Quality Control Process

We conducted further statistical and quality control analyses on the data from the side-by-side operation of the two methane analyzers at LMA during fall 2019, before the second analyzer was permanently moved to LUR. Time series graphs with the recordings of both analyzers overlaid were presented previously in the 2019 Summary Report. A statistical distribution analysis was performed for data recordings during times when the analyzers sampled the same air. Factory calibration settings were used for both analyzers. No post-processing span or offset corrections were applied. The results, in box whisker plot format, are illustrated in Figure SD1. Numerical results are summarized in Table SD1.Very close agreement between the two analyzers was observed. As a matter of fact, this is about the best agreement between two independently running instruments that we have ever observed. Differences between the two analyzers at the different percentile levels are <1 to 2 ppb. At the approximately 2000 ppb absolute methane mixing ratios, this accounts to a relative error of < 0.05 to 0.2%. This excellent agreement between the two analyzers gives high confidence that any differences larger than these margins seen in monitoring data between LMA and LUR are true ambient concentration gradients and not due to instrument biases of either of the two analyzers.

As already described in the Q2 report, during the second to third week of June 2020, the Thermo Scientific analyzer for the monitoring of nitrogen oxides was replaced with a new analyzer from Teledyne (Model T200UP). Both of these analyzers are approved regulatory-grade monitors. Both analyzers were calibrated individually, and the calibration factors were considered in the reported data. The two analyzers were operated side-by-side, sampling the same air at LUR and collected through the same inlet for one week. Results from this monitoring, both as time series and linear regression analyses, are presented in Supplement E. The agreement of the measurements is somewhat variable by day. While the time series plots show an overall very similar dynamical behavior for nitric oxide (NO), the Thermo Scientific analyzer has a lower response, by 10-21%. For NO_2, the deviations in the time series are somewhat larger. The regression line slopes, however, span from both negative (-7%) to positive (+23%) values. There is also an obvious intercept in the relationship, indicating that the Thermo Scientific analyzer is reporting nitrogen dioxide (NO_2) when there was none detected by the Teledyne monitor. As explained in the Q2 report, this difference is likely due to the different conversion

techniques that are applied in the two analyzers. Please note that these offsets were not observed in the calibration measurements where a zero air gas is subjected to the analyzer. A portion, and possibly most of the offset can therefore be explained by other present oxidized nitrogen compounds that are recorded by the Thermo Scientific analyzer as NO_2. In order to bring the record from the two monitors to a more consistent scale, we investigated how the NO_2 background signal that was recorded by the Thermo Scientific analyzer compared to the two other regional NO_x monitors operated at BRZ and BSE. Only data at high wind speeds, when NO_x levels are at consistent and very low levels, were considered. The comparison of the monthly 2-percentile values showed a positive bias of 0.97 to 3.8 ppb for the LUR analyzer (Table SE1). These values have now been applied as best estimate corrections in the LUR January – June NO_2 data in order to bring the NO_2 data recorded during January – June 11 from the Thermo Scientific instrument in closer agreement with actual ambient NO_2. Measurements after June 11 are from the Teledyne monitor that, using a photolytic converter, provides a more 'true' NO_2 measurement, and do not require any such corrections.

5. Website Development

No major changes from the Q2 report. A new website visit counter was implemented. A few updates and corrections were made to the methods and background text.

6. Data Archiving

No Changes from the Q2 report.

7. Data for Quarter 3, 2020

The data that were recorded in Q3, 2020, are included in this report in graphical time series format in Supplement A (LMA) and Supplement B (LUR). These graphs show the completeness of the data coverage and general features in the dynamic, diurnal, and seasonal changes. Some of the data (e.g., wind direction) are difficult to interpret when 3 months of data are included in the same plot. In these instances, the primary objective is to show general trends and that the data are nearly continuous – not to point out individual features. Data coverage for all variables is >95% for the full quarter.

In Supplement C, the variables that are measured at both sites are shown together in a set of time series graphs. These graphs are presented to highlight similarities and differences between the LMA and LUR monitoring locations.

8. Selected Data Examples and Preliminary Interpretations

Meteorology

A remarkable and highly unusual change in meteorological conditions occurred on September 8-9, when temperatures dropped from above 30°C to near freezing the next day (Figures SA1 and SB1). This change was associated with a cold front moving into the region from the north. Interestingly, this weather

change also caused very obvious changes in air pollutant concentrations. Notable drops in concentrations were observed across all monitored species, including ozone.

Ozone

Figure 1 presents an interesting case study analysis of an event that happened on July 10. This was during a period when elevated ozone was observed almost daily. July 10 was a unique situation, however. After a rapid increase in ozone during the morning hours, as typical during summer days, there was a sudden drop in ozone shortly after noon. This drop was seen at both Longmont sites, as well as at BRZ (Figure 1). The wind data included in Figure 1 show how this sudden reversal of the morning ozone increase was associated with a change in the air flow. While air was being brought into the area from the east during the morning, around 1 p.m. winds shifted to the west. This flow change, with air coming from over the mountains to the Front Range, lasted approximately three hours. Ozone dropped in an instant by ~20 ppb, and kept declining during the following hours. The air transport then very suddenly reverted back to easterly flows around 5 p.m. The flow reversal was again associated with a remarkable change in surface ozone, but this time with an increase. Ozone increased by 30 ppb at LUR within less than half an hour, briefly reaching a maximum of 84 ppb. In summary, this event clearly showed the different ozone chemistry and resulting ozone maxima related to a change in air mass. Air moving in from the west was much lower in ozone, with daytime levels around 50 ppb. In contrast, air transported from the east during that day was 30 ppb higher in ozone. If there hadn't been this midafternoon flow reversal, the observed morning rise in surface ozone would have likely resulted in a midday exceedance of the 8-hour ozone NAAQS. The air transported from the west resulted in an 8-hour average ozone well below the standard.

In Figure 2, all ozone data for the months of May through August were associated to concurrent wind data to generate wind dependency 'heat maps' that show the average ozone as a function of wind speed and wind direction. This analysis was done for LMA, LUR, BRZ, and BSE. While there are some slight differences in the heat maps between the sites, there is a consistent finding: For all sites, the predominant source region for high ozone conditions ranges from the north to the southeast of these monitoring sites.

The full Q3 ozone records for LMA and LUR are presented in Figures SA8 and SB8. Overall, ozone was higher in Q3 compared to Q2. Elevated ozone was observed during the month of August, with the highest values for the full year. The 8-hour averaged ozone plotted in Figures SA9 and SB9 allow an easy comparison of recorded ozone with the NAAQS. At LMA, the 70 ppb ozone NAAQS was exceeded on two days in July, and on six days in August. At LUR, there was one exceedance in July, and nine exceedances in August. The overall highest 8-hour ozone, 83 ppb, was observed at LUR on August 24.

Several of the high ozone days occurred on days when the Front Range was subjected to wildfire smoke. This dependence is investigated in Figure 3. The lower graph identifies smoke conditions using the 24-hour PM_2.5 data as the indicator. Heavy smoke days are bracketed by the vertical red lines. During the first smoke episode that lasted five days, ozone was quite elevated, with the 8-hour ozone exceeding the NAAQS on every single day. This may suggest that pollutants transported with the fire smoke plumes were a cause of this ozone increase. This hypothesis is not supported, however, by the following three smoke events - ozone on those days wasn't nearly as elevated. In contrast, during the last smoke event, the 8-hour ozone was comparatively low, not exceeding 50 ppb. In summary, while there is an indication that the polluted air resulting from the fires may have contributed to elevated ozone, a causal association is not clear based on the lack of the correlation during many other days.

Figure 4 presents a statistical analysis of the full Q3 ozone data, comparing the Longmont data with observations from BRZ and BSE. This analysis illustrates the increase in ozone heading into the later summer months, with a subsequent decline in September. Figure 4 also shows that ozone levels in Longmont were slightly lower than at the comparison sites, which is a trend consistent with observed ozone levels during the preceding quarters.

CO_2

The full Q3 CO_2 records are available in Figures SA6 and SB6 for LMA and LUR, respectively. Mole fractions of CO_2 during Q3 exhibited similar levels as in Q2. Figure 5 shows how the median CO_2 values, illustrated by the black line in the middle of each colored box, are within a relatively narrow range and remained relatively consistent during all three months in Q3. The wind dependency analyses in Figure 6 illustrate that the dominant CO_2 contributions are from the west at low wind speeds. These results are very similar to the ones reported in Q2. Since the LUR site is east of the City of Longmont, this suggests that the city is the primary source for enhanced CO_2 observed at LUR. However, as already mentioned in the Q2 report, the cause for the high CO_2 mole fractions seen in winds from the west of LMA is unclear and will need to be further investigated.

Methane

The full Q3 methane records are available in Figures SA7 and SB7 for LMA and LUR, respectively. Figure 7 also shows that both LMA and LUR recorded more variability and larger values at the higher percentile margins than at the BRZ and BSE sites in the neighboring cities. LUR Q3 median values of methane tended to trend slightly upward over the three months. Figure 7 also shows that LUR recorded more variability and larger values at the higher percentile margins. Among the two Longmont sites, LUR in particular, has higher absolute values and variance when compared with LMA. This is likely the result of its proximity to the oil and gas operations east of the city. Figure 8 supports this proximity argument as it shows high values of methane primarily coming from the northeast sector at LUR. LMA shows a wider distribution of prominent methane sources, with a relatively stronger contribution from the north.

VOCs

The full Q3 LUR records for seven selected VOCs are available in Figures SB10–SB16. During Q3, we saw a similar trend as for the Q2 data, with a significantly diminished frequency of elevated VOCs events compared with Q1 of 2020 (Figure 9). The time series plot, including the comparison data from BRZ, BSE, and BLV, indicates that there may be a slight increase in frequency of VOCs spikes occurring again, compared to April –June, towards the latter part of the record. This impression is confirmed by the statistical analysis of the data (Figure 11). For the oil and gas tracers ethane and propane, the higher percentile values at LUR appear to be increasing at higher rates than at BRZ and BSE. This behavior is not quite as obvious for benzene, however.

A remarkably high concentration sample was collected on August 12, with a sampling time of 19:30 to 19:40 hours. Ethane was quantified at 260 ppb. Other oil and gas tracers were similarly enhanced (Figure 10), with many of them quantified at levels 100 times above the regional background. This sample has a very clear oil and gas signature, with light alkanes being the dominant VOCs. The wind speed was low when this event was picked up by the sensors; the wind direction was coming almost directly from the south. In previous quarters we have not seen a signature such as this one, with highly

elevated VOCs originating in air transported from the south; as of right now this appears to be an interesting anomaly to investigate in the future. Figure 12 paints a somewhat blurrier image of VOCs average dependence on wind conditions at LUR than what we have seen in previous quarters. Ethane and propane show a somewhat wider spread of source sectors to the north. Benzene and acetylene are mostly associated with the City of Longmont upwind direction. The wind direction dependency for benzene and acetylene is more clearly defined in Q3 compared to Q2 findings. The correlation analyses in Figure 13 indicates that benzene, in particular, is less obviously correlated with propane and ethane compared with Q1 and Q2. The VOCs ratio plots in Figure 14 are not quite as distinct as in Q2, but nonetheless have the same general signatures as discussed previously. Figure 15 presents a similar correlation analysis for the wildfire smoke plumes as presented for ozone above, using benzene as a VOCs fire smoke tracer. There is a notable increase in benzene during the peak of the smoke events. This behavior is consistent among the four VOCs monitoring sites. The increase in benzene in the smoke plumes is on the order of 100 – 300 ppt. These enhancements are well below the benzene increases that are seen frequently in the oil and gas plume spikes. The similarity seen in the data from the four sites illustrates a relative homogeneity in the smoke plume distribution that was present in the Colorado Front Range.

Nitrogen Oxides (NO, NO_x)

The Q3 LUR record for NO is available in Figure SB17, and the record for NO_x in Figure SB18. Results are similar to Q2. Both NO and NO_x mole fractions are higher at LUR than at sites in neighboring cities (see Figure 16). A striking feature is the large increase for the higher percentile values at LUR, and how this difference increased steadily in the weeks before autumn. The City of Longmont appears to be the strongest upwind source for both NO and NO_2 (Figure 17).

Particulate Matter (PM)

PM10 and PM2.5 LUR Q3 monitoring results are presented in Figure SB19 and SB20. During August and September, concentrations of both PM 10 and PM 2.5 were on average significantly higher than values recorded during Q2 (Figure 18). There is a remarkable agreement in the temporal behavior and recorded absolute values between BSE and LUR. This is a clear indication that the PM occurrences were a large-scale geographical phenomenon. As already discussed in the preceding sections, the enhanced particulates resulted mostly from wildfire smoke plumes that were transported into the Front Range from fires within the state as well as from the U.S. West Coast (Figure 19). These smoke plume events resulted in many days with severely degraded air quality. To most citizens, the poor air quality was noticeable by the persistent smoky haze and the smell of burning material. The 24-hour PM2.5 NAAQS of 35 $\mu g\ m^{-3}$ was exceeded on ten days total. The highest value was measured on September 17 with 53.5 $\mu g\ m^{-3}$.

Figures

A

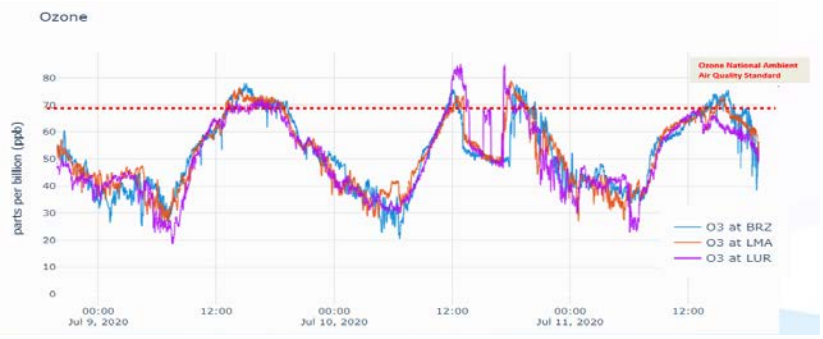

B

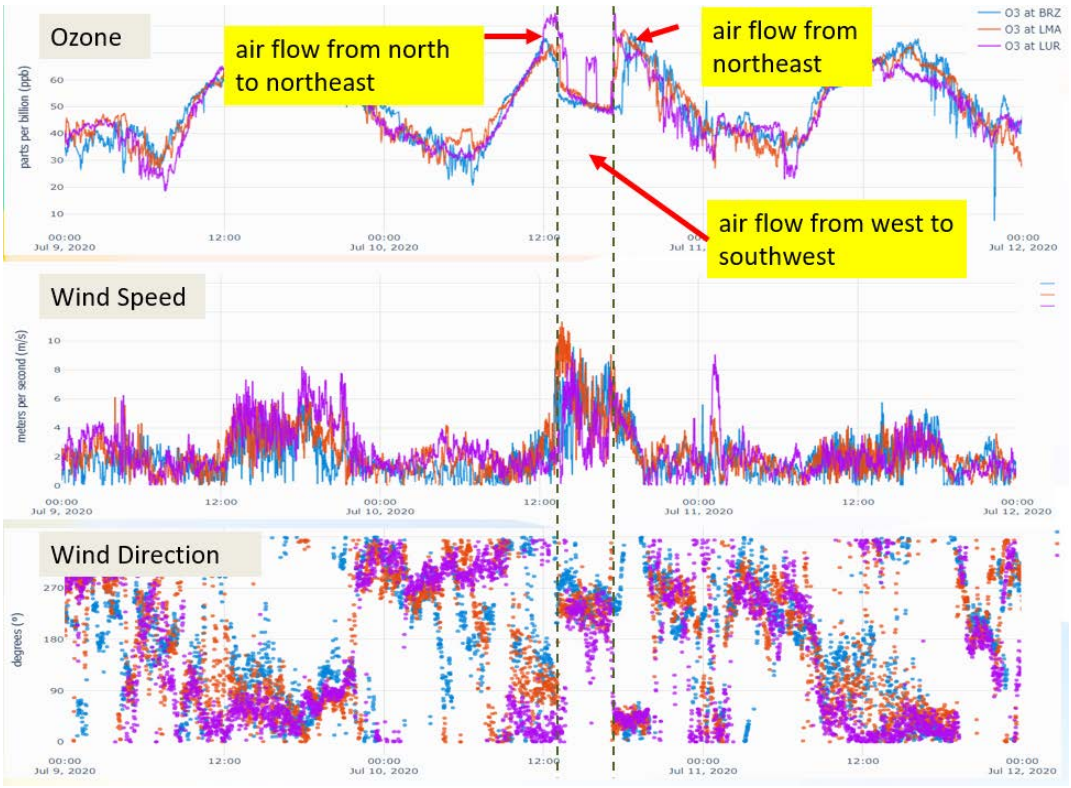

Figure 1:
Notable ozone event on July 10, 2000. The upper graph (A) shows the ozone recordings from Boulder Reservoir (BRZ), LMA, and LUR. They all show a similar behavior on these three days when ozone exceeded the 8-hour NAAQS on each day. On July 10, there was a sudden dip in the diurnal ozone cycle around noon. This behavior was seen at all three sites. The lower panel (B) shows the ozone record together with the wind speed and wind direction recordings. This comparison clearly shows that the ~20 ppb ozone drop occurred during a short episode when the wind shifted from northeasterly to west/southwest. The sudden shift in wind direction back to northeasterly, at approximately 3 p.m., reversed the ozone conditions, causing a sudden increase in ozone back to levels well above the NAAQS.

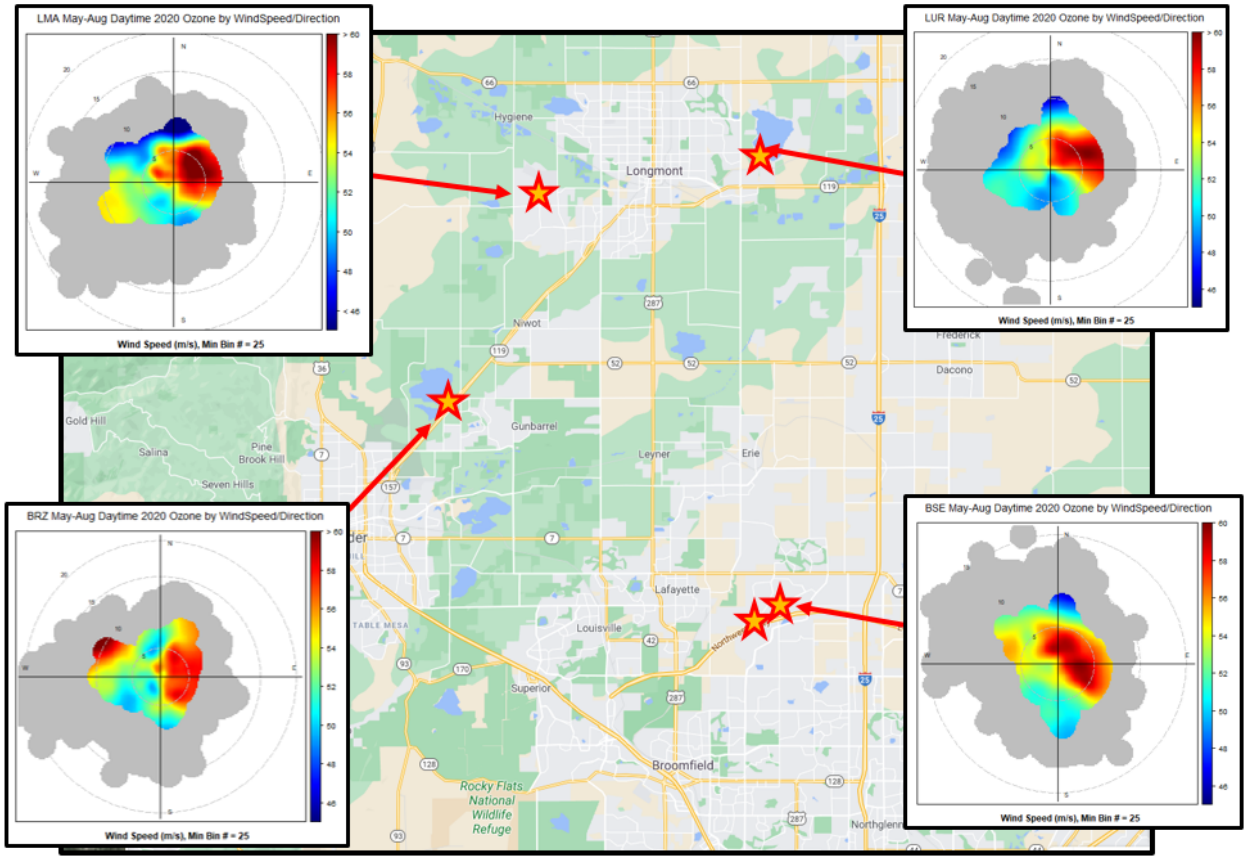

Figure 2:
Analysis of the dependence of ozone levels on wind direction and wind speed for all four network sites, BRZ, LMA, LUR, and Broomfield Soaring Eagle (BSE). These analyses show a consistent picture: High ozone is mostly transported to the monitoring sites from the northeast to southeastern sectors.

Figure 3:
8-hour running mean ozone during July – September at the four network sites (A). The lower graph (B) shows the 24-hour mean PM2.5 analyses from LUR and BSE. Periods with increased PM2.5, resulting from wildfire smoke, are bracketed by the red vertical lines. During the 5-day wildfire smoke window from August 20-25, ozone was elevated, exceeding the ozone NAAQS on every day. In contrast, during the three other smoke events, ozone did not increase to levels higher than measured on no-smoke days. While there is an indication that the polluted air resulting from the fires may have contributed to elevated ozone, a causal association is not clear based on the lack of the correlation during many other days.

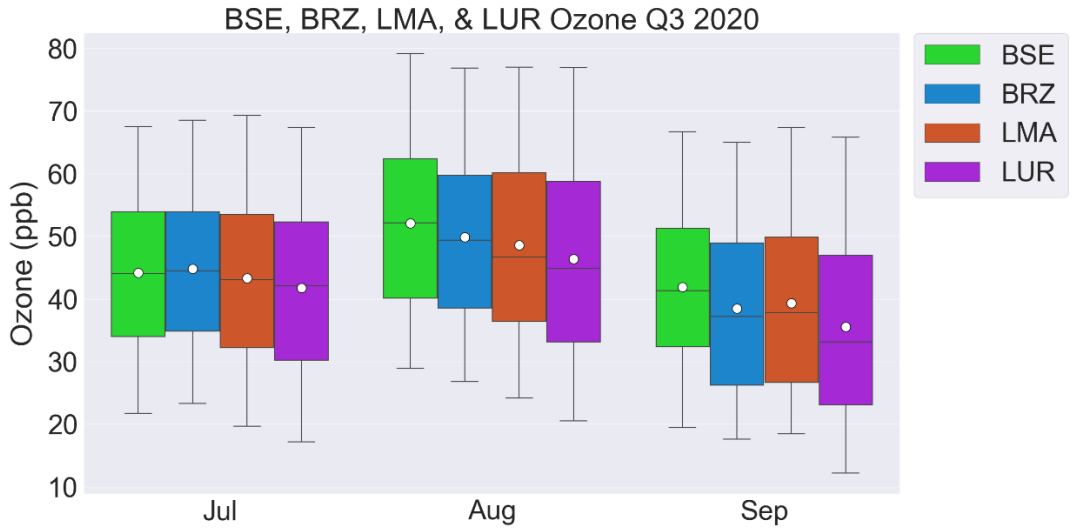

Figure 4:
Comparison of the ozone distribution at BSE, BRZ, LMA, and LUR during July – September 2020. These box whisker plots show the median value as the center line, the 25-75 percentile distribution as the colored boxes, and the 5-percentile and 95-percentile values as the whiskers. The white dot on each box illustrates the mean value at each site. The data illustrate the increase in ozone heading into the later summer months, with a subsequent decline in September. Ozone levels in Longmont were slightly lower than at the comparison sites, which is a trend consistent with observed ozone levels during the preceding quarters.

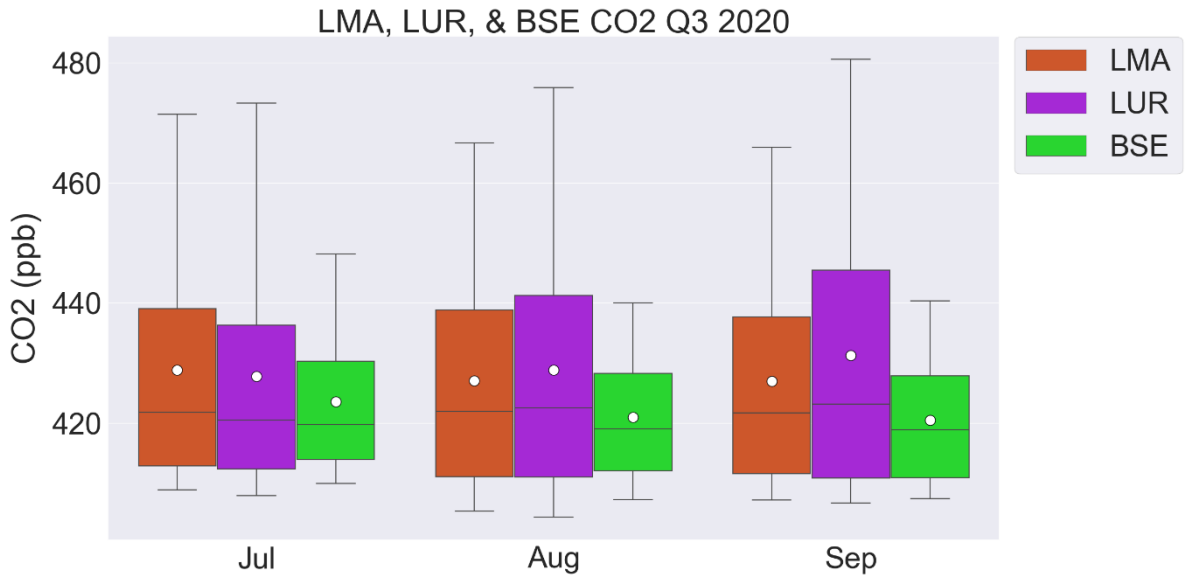

Figure 5:
Comparison of the CO_2 distribution at LMA, LUR, and BSE during July – September 2020. See Figure 4 for explanation of the box whisker plot format. Median CO_2 values, illustrated by the black line in the middle of each colored box, are within a relatively narrow range and remained relatively consistent during all three months in Q3.

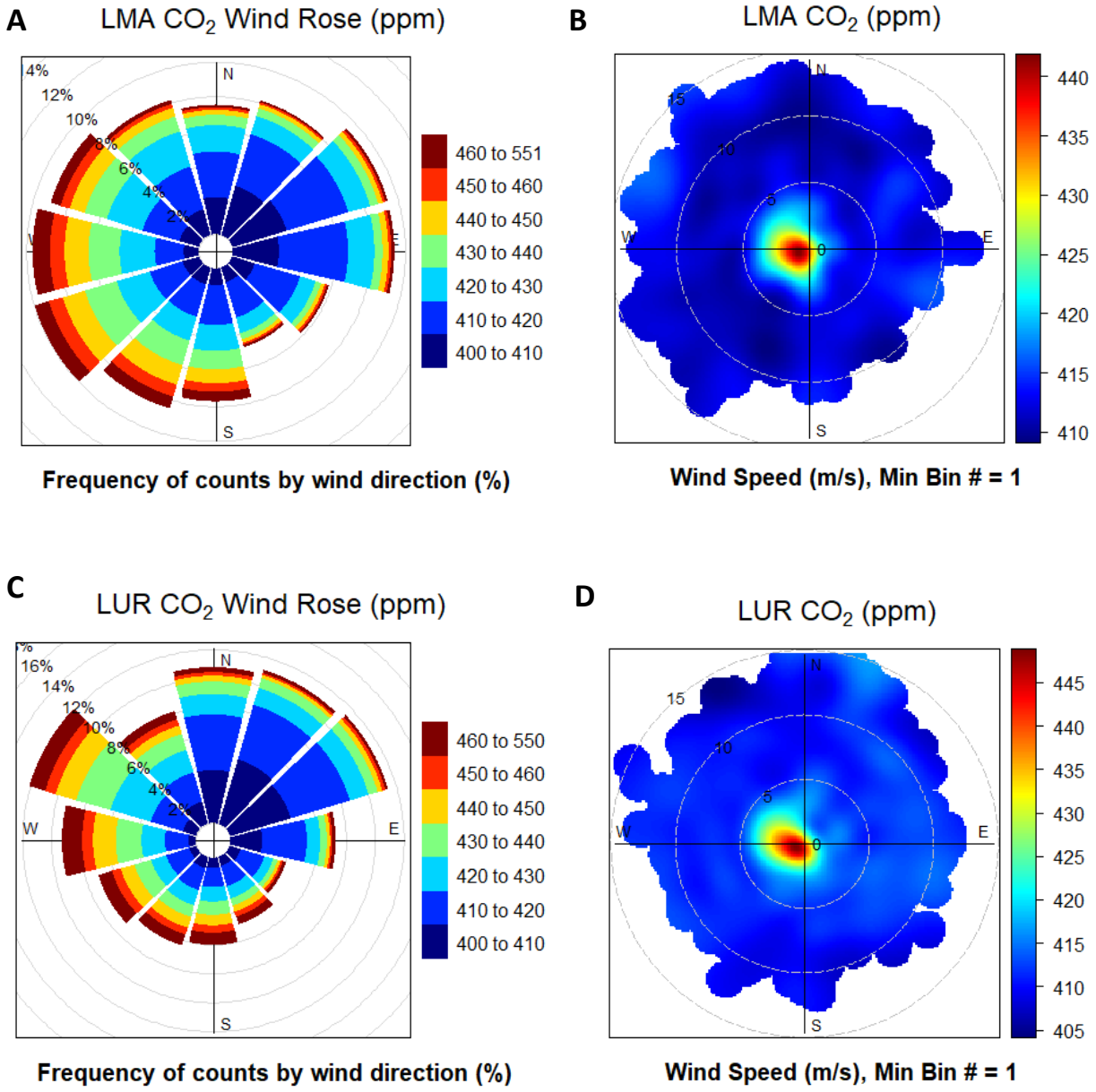

Figure 6:
Wind rose (left) and wind heat map analysis (right) showing the dependency of CO_2 mole fractions at LMA (top, A, B) and LUR (bottom, C, D) during July – September 2020. For both monitoring locations, the dominant CO_2 contributions are from the west at relatively low wind speeds. These results are similar to the ones reported in Q2. Since the LUR site is east of the City of Longmont, this suggests that the city is the primary source for enhanced CO_2 observed at LUR. The cause for the high CO_2 mole fractions seen in winds from the west of LMA is unclear and will need to be further investigated.

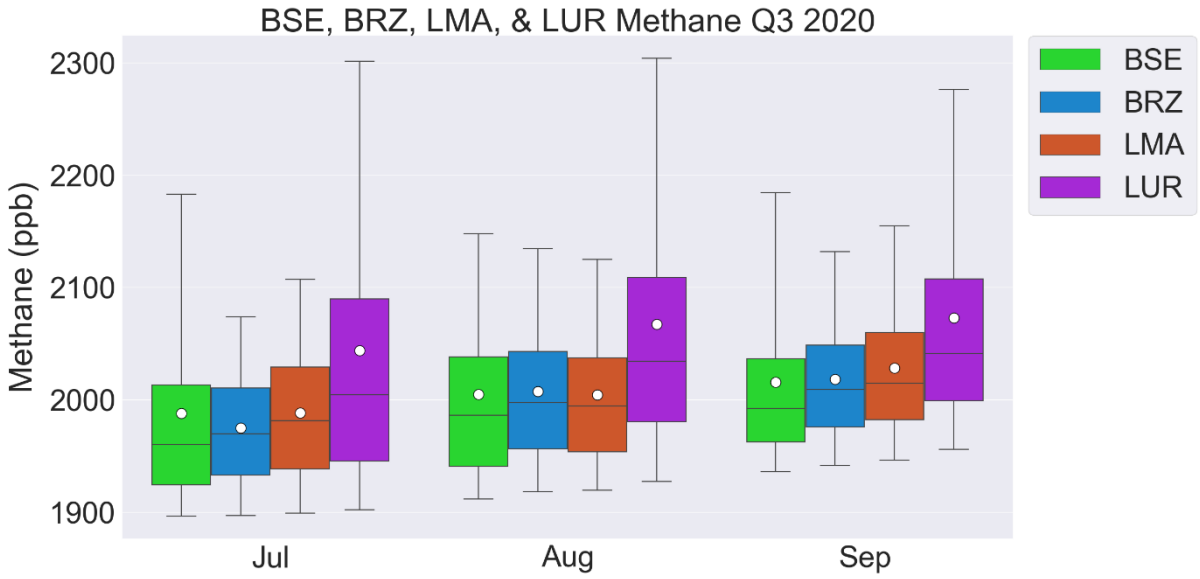

Figure 7:
Comparison of the methane distribution at BSE, BRZ, LMA, and LUR during July – September 2020. See Figure 4 for explanation of the box whisker plot format. LUR recorded more variability and larger values at the higher percentile margins. Among the two Longmont sites, LUR has higher absolute values and variance when compared with LMA.

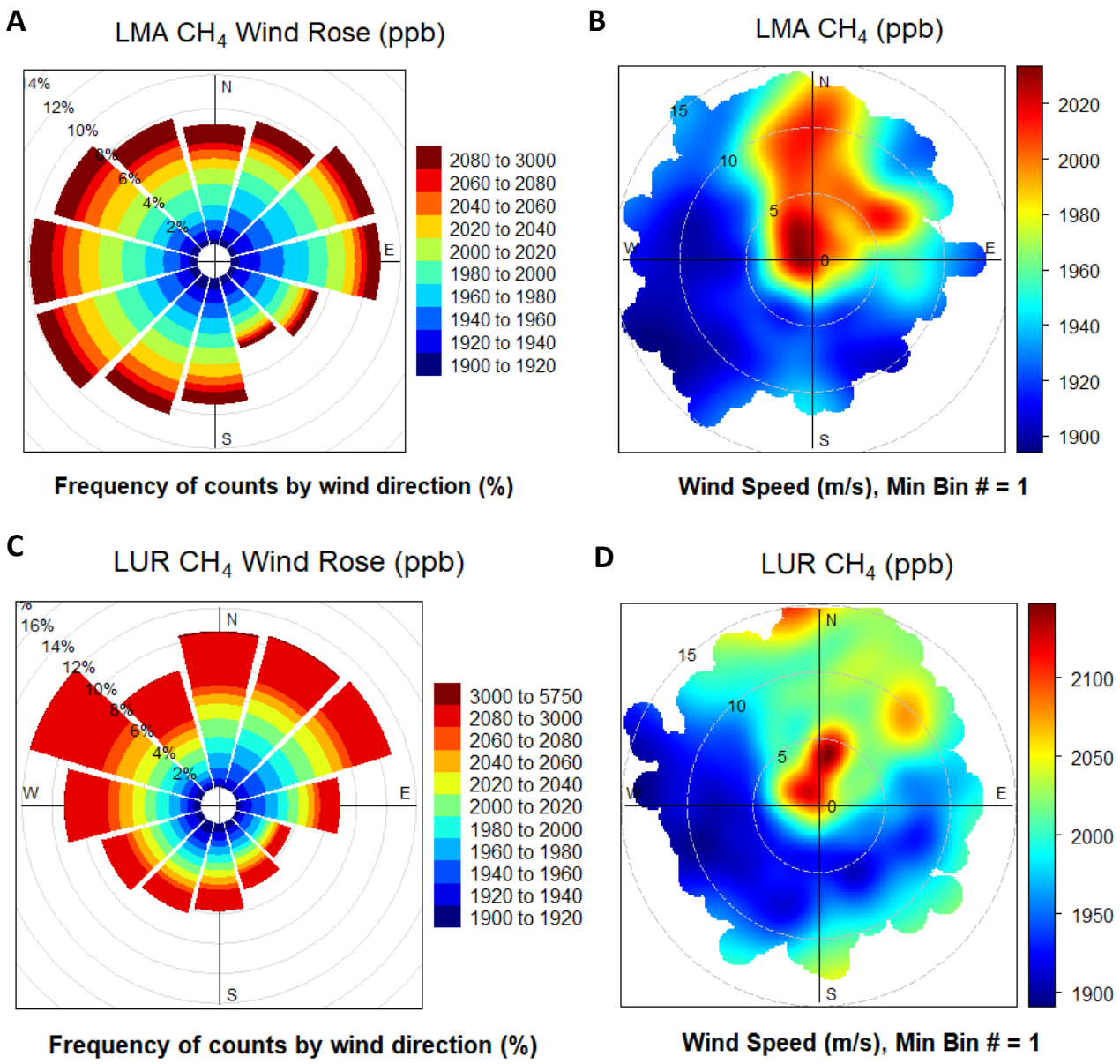

Figure 8:
Wind rose (left, A, C) and wind heat map analysis (right, B, D) showing the dependency of methane mole fractions at LMA (top) and LUR (bottom) during July – September 2020. High methane values are primarily coming from the northeast sector at LUR. LMA shows a wider distribution of prominent methane sources, with a relatively stronger contribution from the north.

Figure 9:
Comparison of ethane at BRZ, LUR, BSE, and BLV during January – October 2020. The lower graph (B) is an enlargement of the 0-50 ppb range from the upper graph (A). The high frequency of high concentration ethane spikes observed at LUR during February to April subsided during late spring and summer. Similar concentration ranges and frequency of spikes were observed during May –August. There is possibly a slight increase in the LUR ethane spikes in the fall again.

A

B

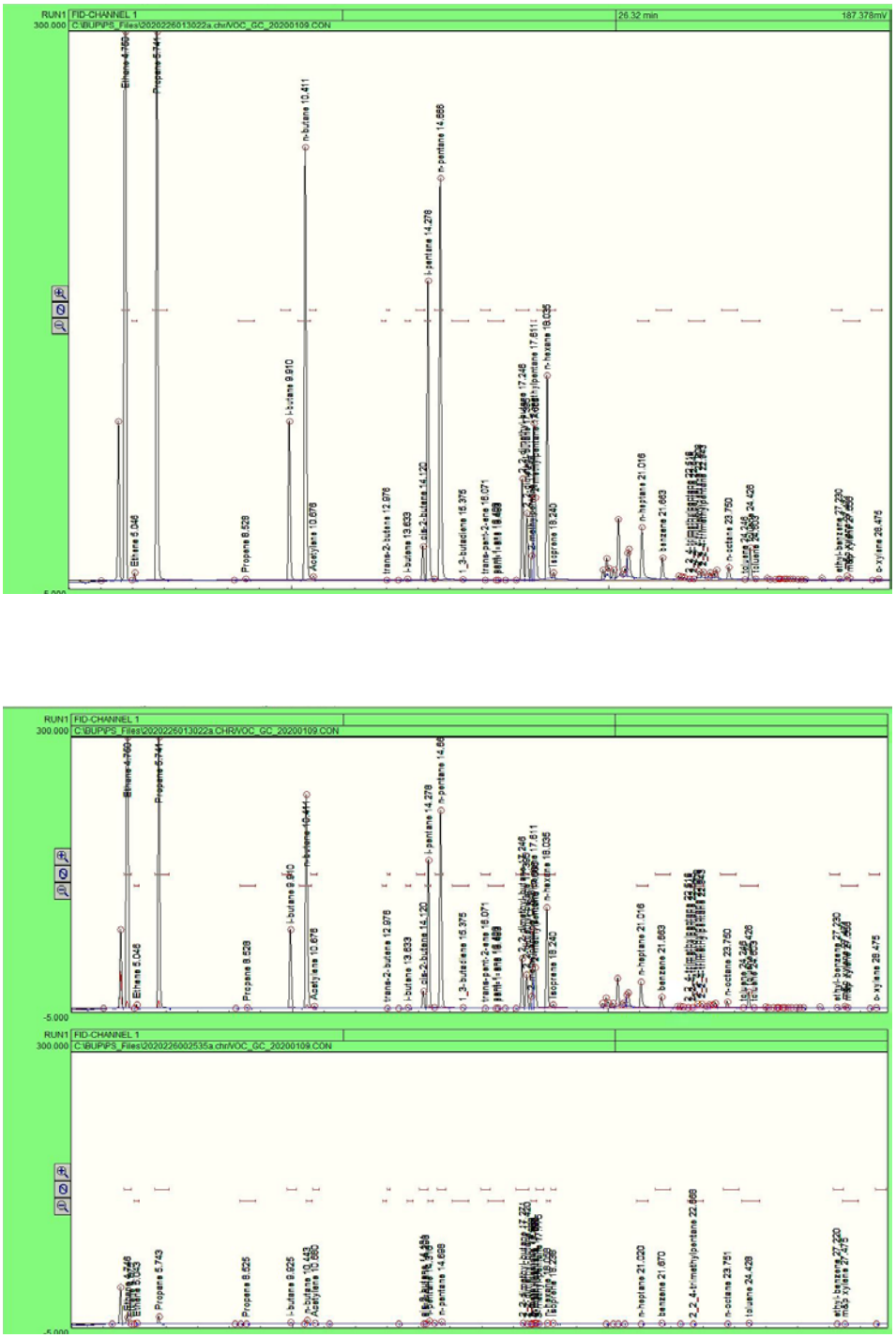

Figure 10:
Gas chromatogram of the highest VOCs concentration sample seen during Q3 on August 12, 2020. The upper graph (A) shows the full chromatogram, with peaks labeled. Ethane was quantified at 260 ppb, which is more than 100 times the regional background. The bottom window (B) shows the same chromatogram again as the upper trace, with a sample run right before this spike plotted underneath. This comparison shows the stark contrast in the number of peaks and concentrations, represented by the height of the peaks, between these two consecutive samples.

A

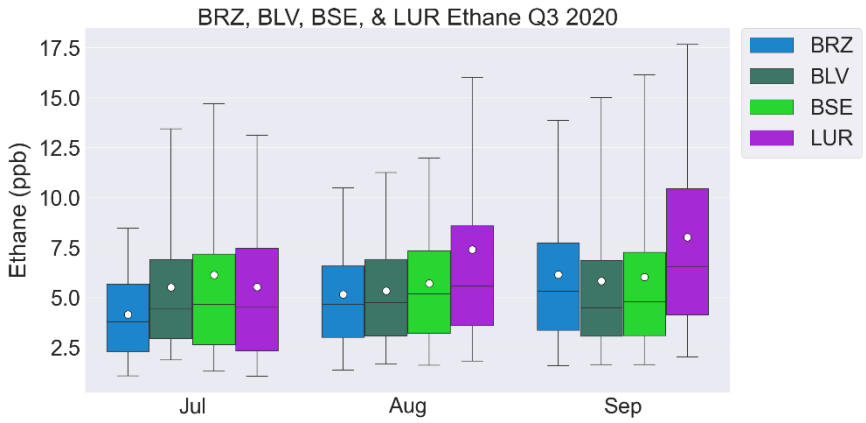

B

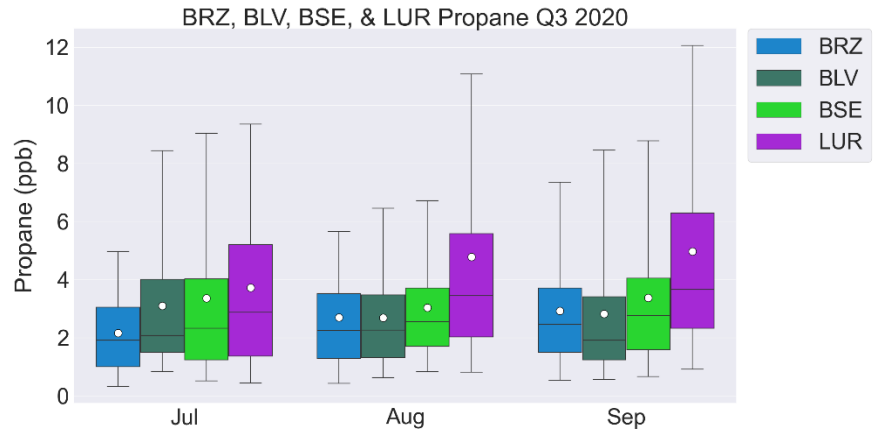

C

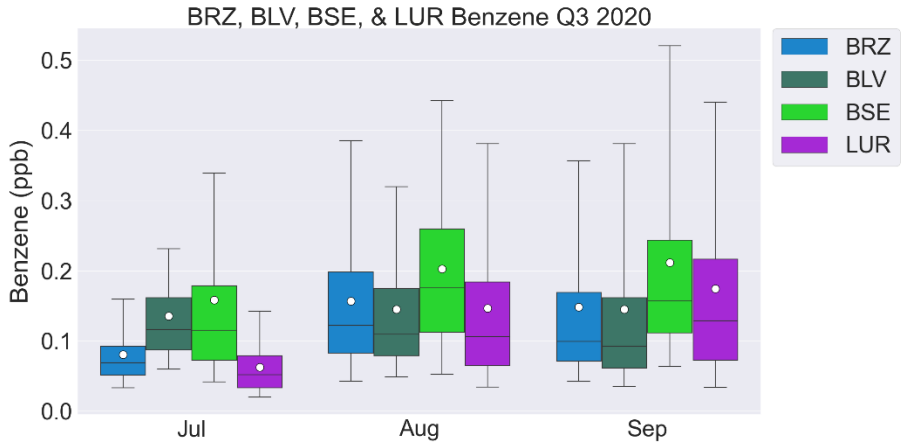

Figure 11:
Comparison of the distribution of ethane (A), propane (B), and benzene (C) at BRZ, BLV, BSE, and LUR during Q3. See Figure 4 for explanation of the box whisker plot formats. For the oil and gas tracers ethane and propane, the higher percentile values at LUR appear to be increasing at higher rates than at BRZ and BSE. This indicates that there may be a slight increase in frequency of VOCs spikes occurring again, compared to April – June. This behavior is not quite as obvious for benzene.

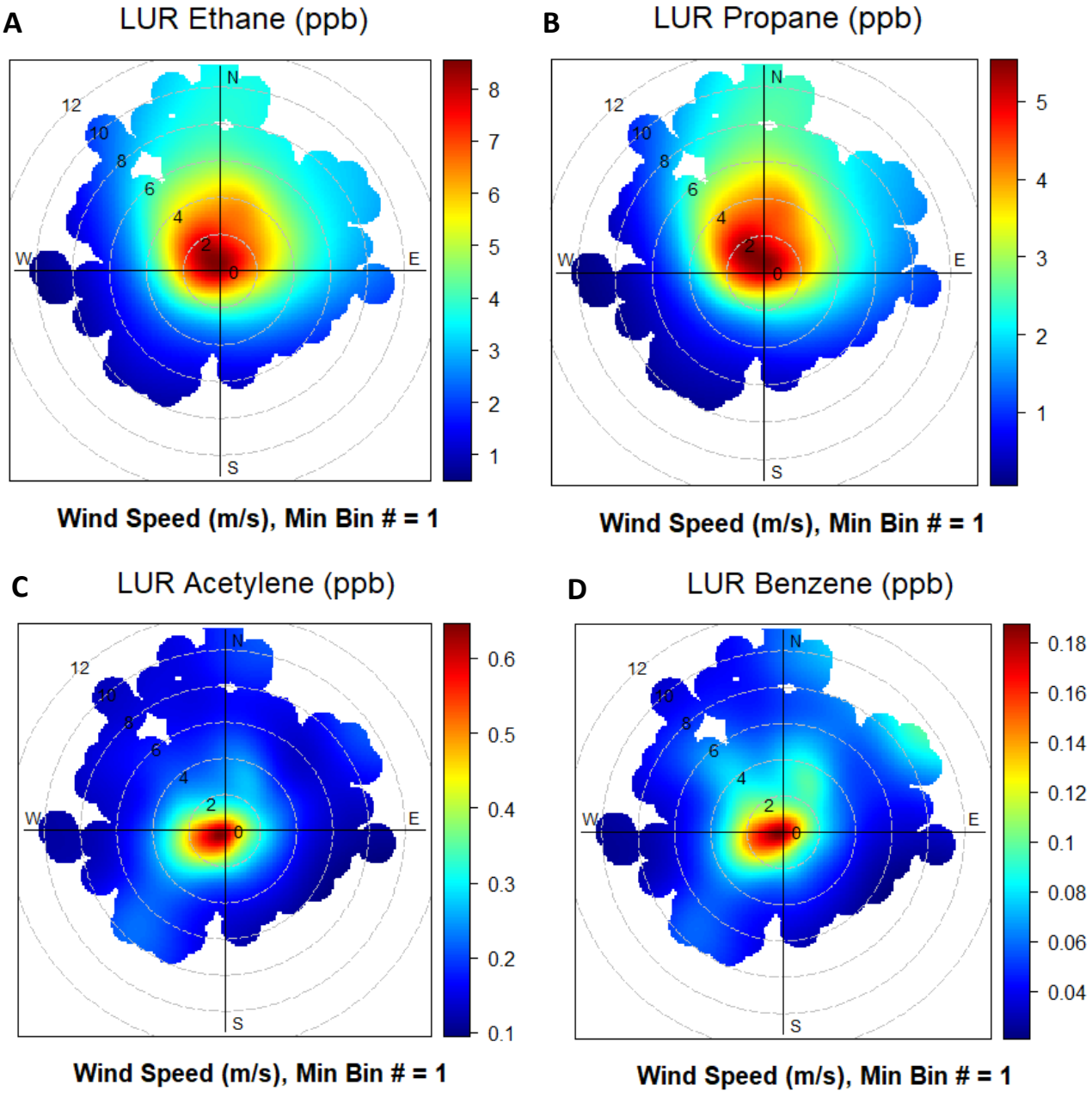

Figure 12:
Comparison of ethane (A), propane (B), acetylene (C), and benzene (D) occurrences as a function of wind speed and direction at LUR during Q3. Ethane and propane show a somewhat wider spread of source sectors to the north. Benzene and acetylene are mostly associated with the City of Longmont upwind direction.

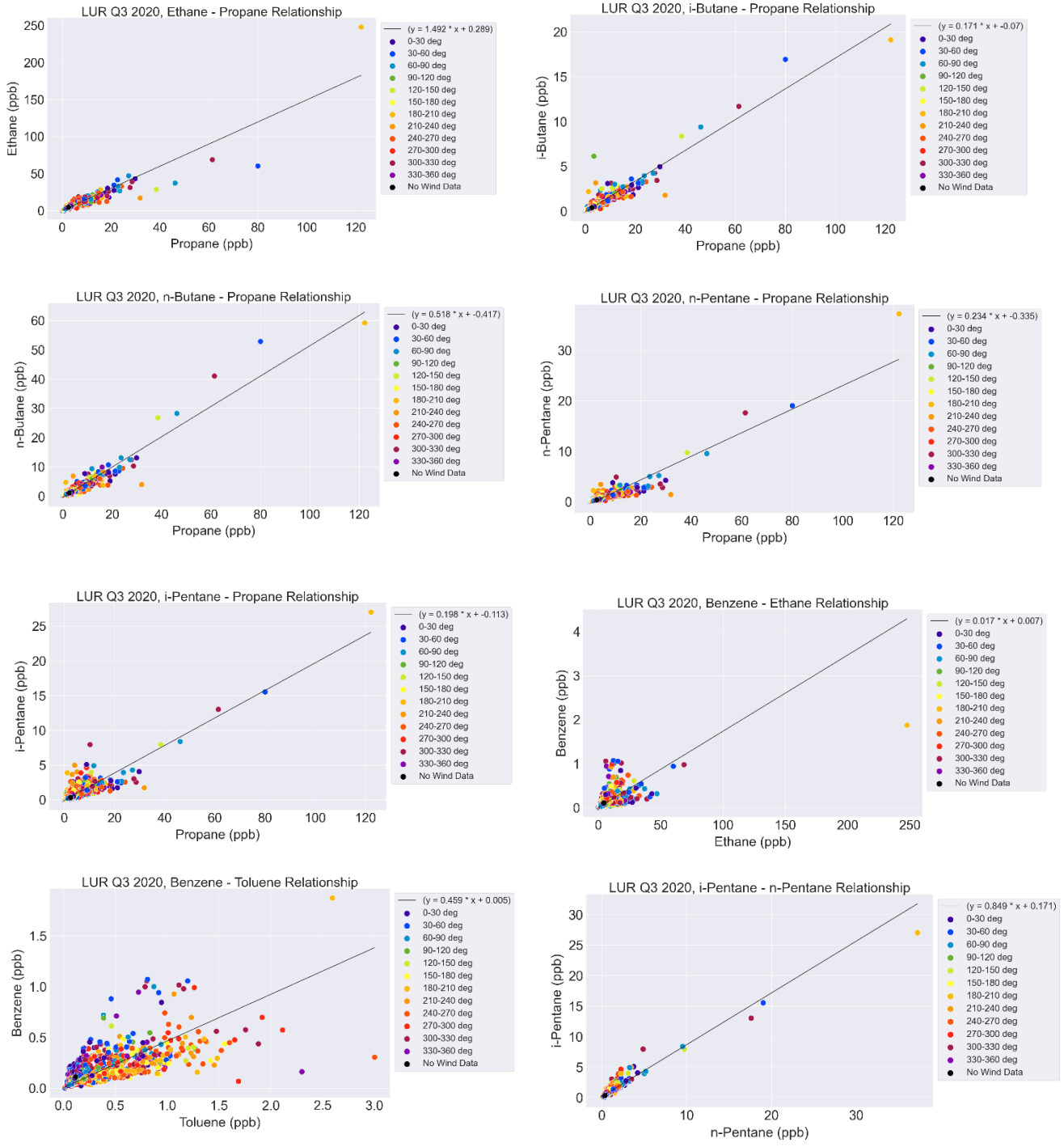

Figure 13:
VOC-VOC relationships at LUR during Q3. Data points are color coded by wind direction. The black line is the result of an orthogonal linear best fit regression calculation.

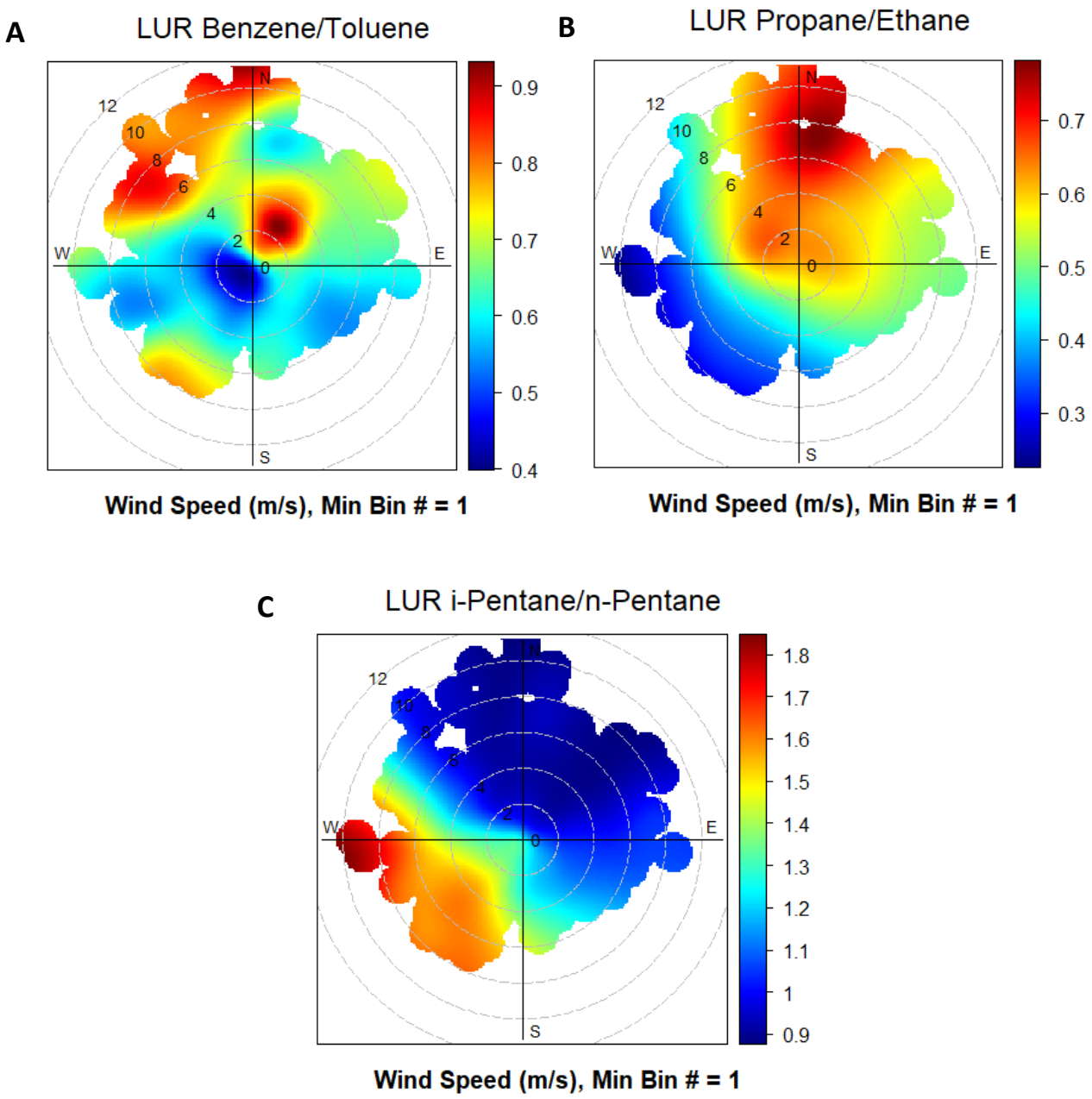

Figure 14:
Ratios of selected VOC pairs as a function of wind direction and wind speed during Q3. These dependencies are not quite as distinct as in Q2, but nonetheless have the same general signatures as discussed for the Q2 data previously.

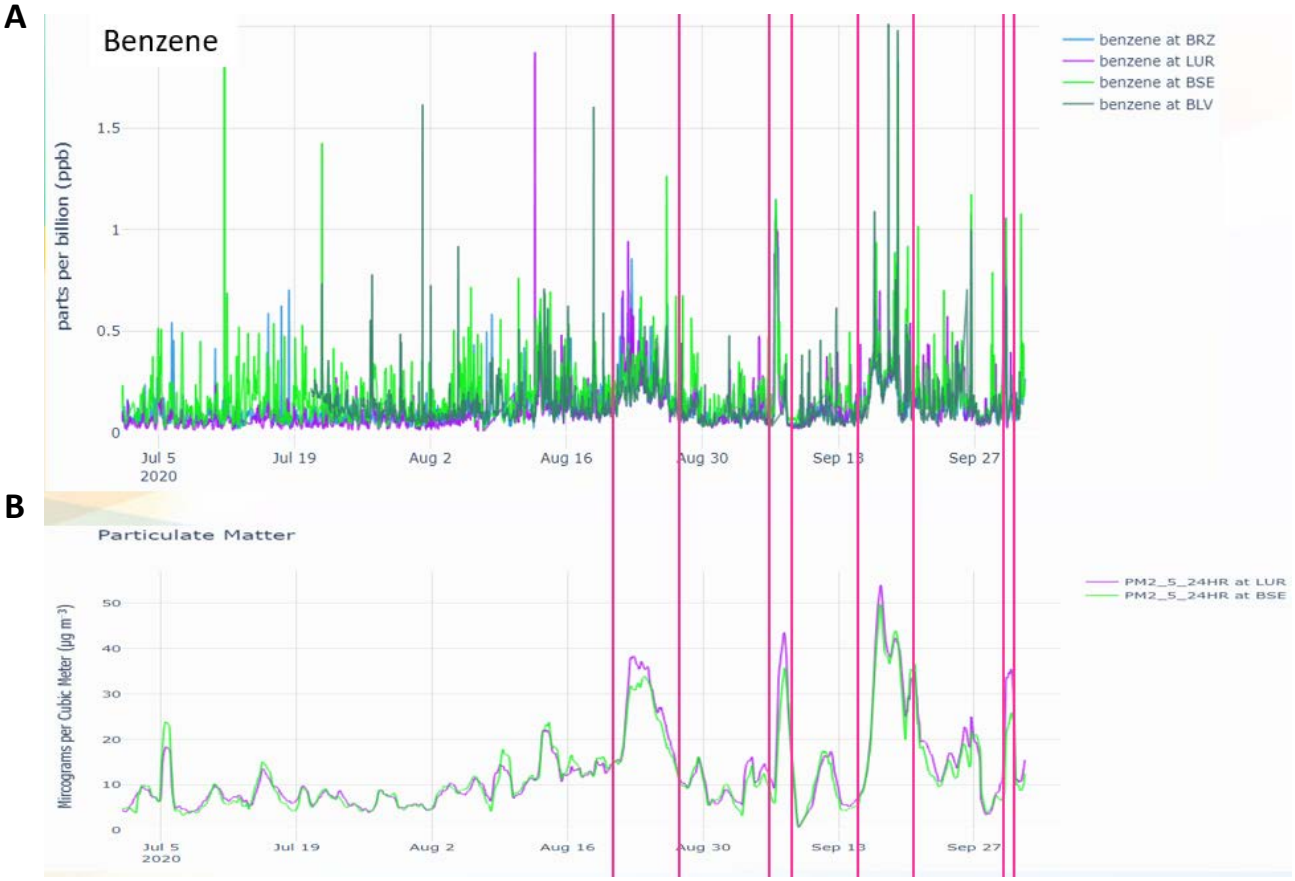

Figure 15:
Comparison of the benzene records (A) with the wildfire tracer PM2.5 (B), similar to the analysis shown in Figure 3 above. There was a notable increase in benzene during the wildfire episodes. This behavior is very consistent among the four monitoring sites. The increase in benzene in the smoke plumes is on the order of 100 – 300 ppt. These enhancements are well below the benzene increases that are seen frequently in the oil and gas plume spikes.

A

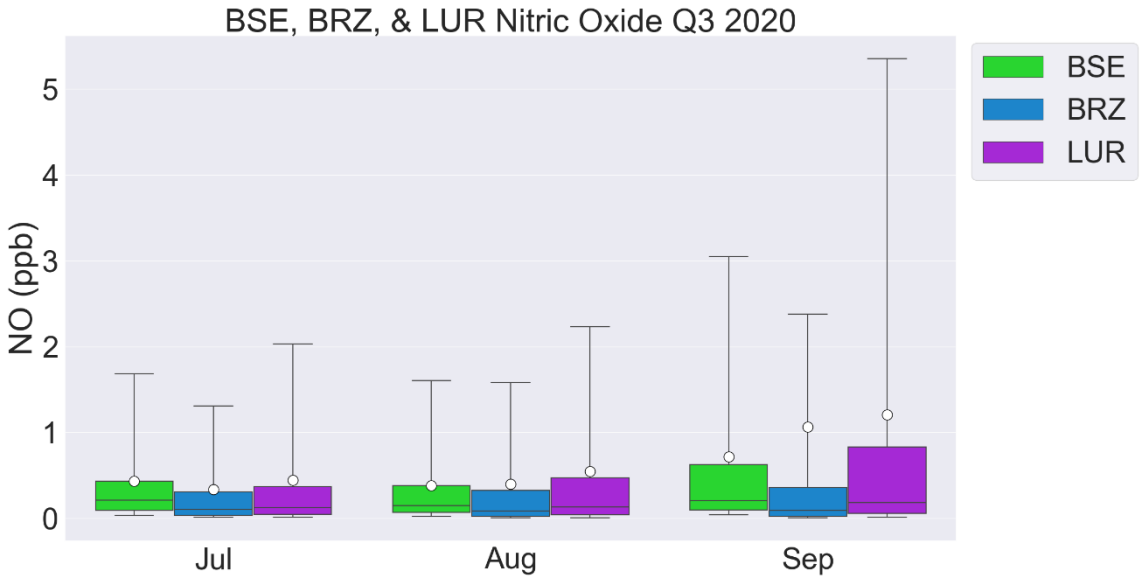

B

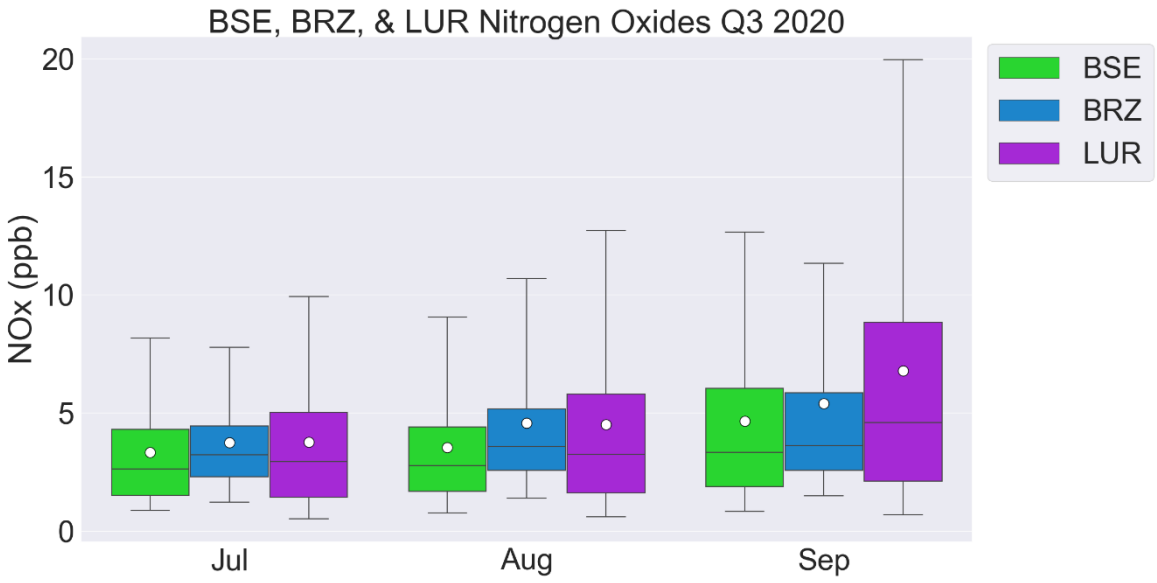

Figure 16:
Comparison of nitric oxide (A) and nitrogen oxides (B) at BSE, BRZ, and LUR during July – September 2020. See Figure 4 for explanation of the box whisker plot formats. Both NO and NO_x mole fractions are higher at LUR than at sites in neighboring cities. A striking feature is the large increase for the higher percentile values at LUR, and how this difference increased steadily in the weeks before autumn.

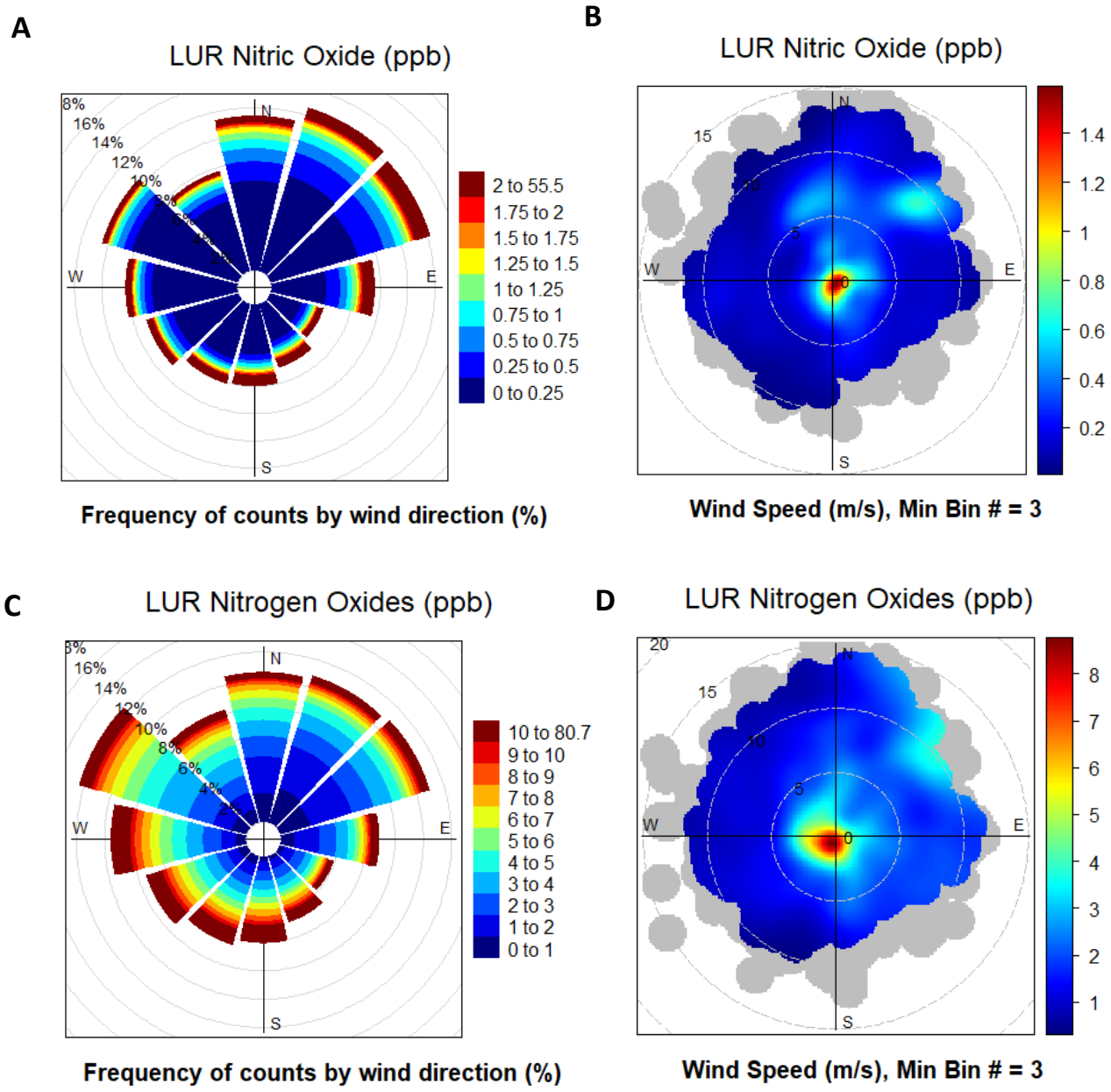

Figure 17:
Dependence of nitric oxide (A, B) and nitrogen oxides (C, D) as a function of wind speed and direction at LUR during July – September 2020. The City of Longmont, located to the west, appears to be the strongest upwind source for both NO and NO_2.

A

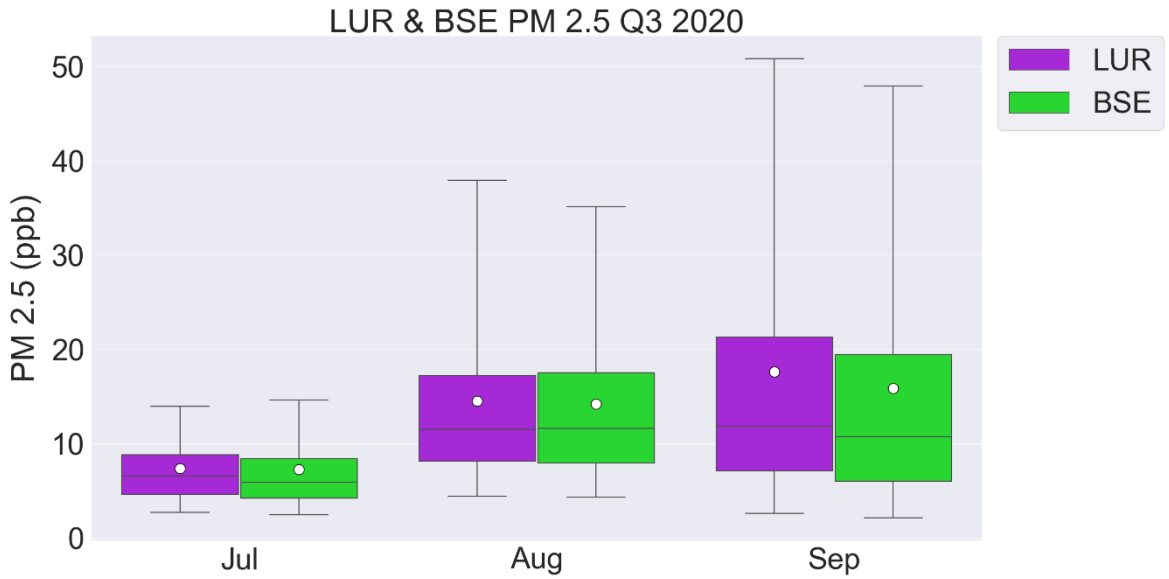

B

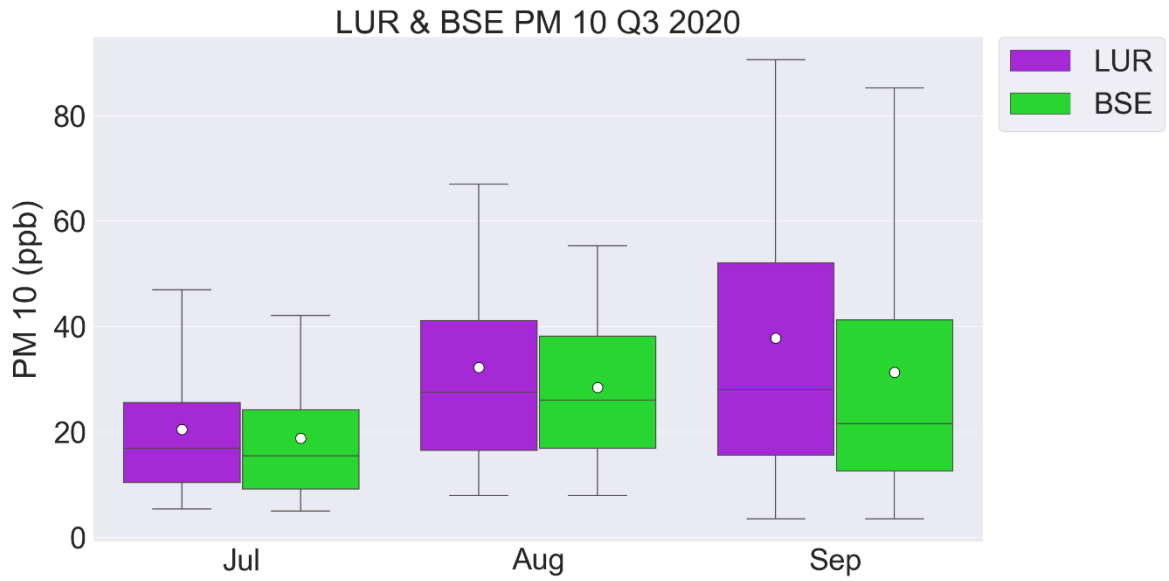

Figure 18:
Comparison of PM 2.5 (A) and PM 10 (B) at LUR and BSE during July – September 2020. See Figure 1 for explanation of the box whisker plot formats. During August and September, concentrations of both PM 10 and PM 2.5 were on average significantly higher than values recorded during Q2, largely due to the occurrences of wildfire smoke events. There is a remarkable agreement in the temporal behavior and recorded absolute values between BSE and LUR.

A

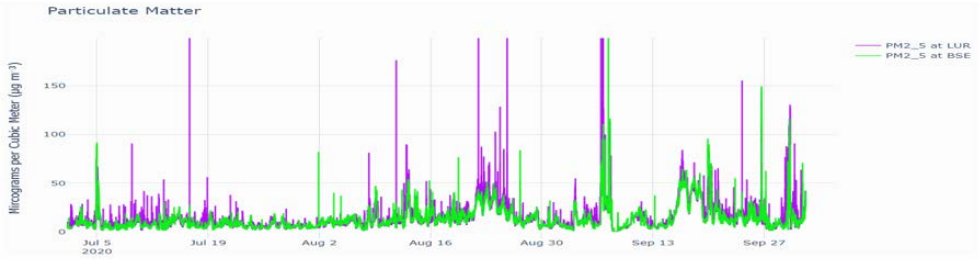

B

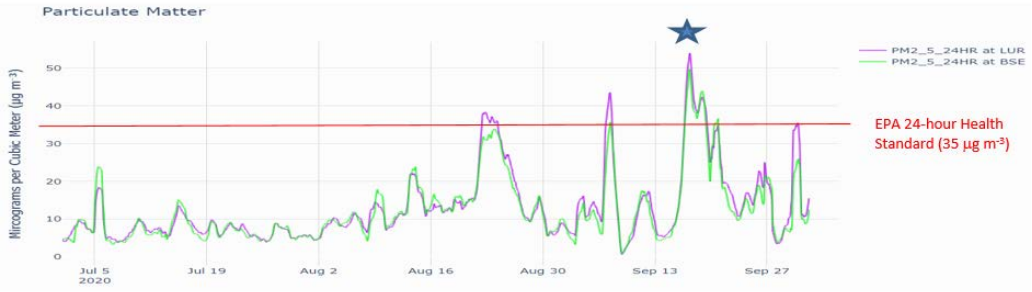

C

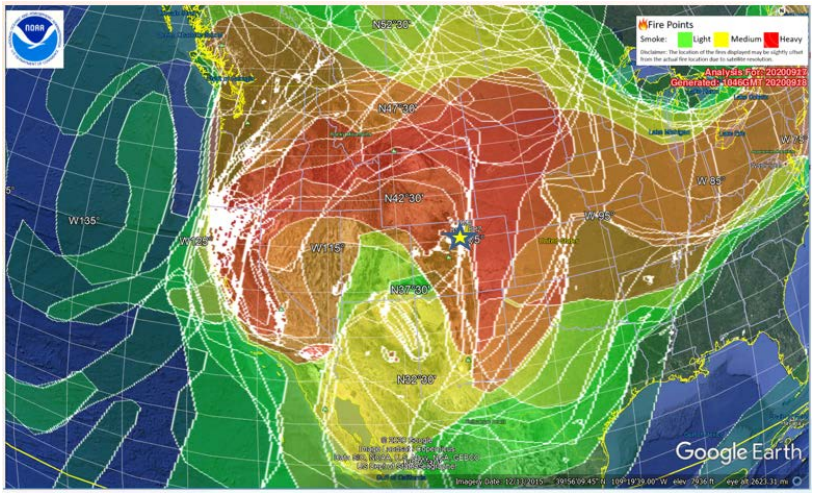

Figure 19:
High time resolution (A) and the regulatory metrics, i.e. 24-hour averaged PM2.5 data, below (B), from both BSE and LUR. Very similar patterns are seen in the data from both sites. The averaged data agree within 10% during most times, indicating that PM2.5 levels were mostly homogeneously distributed across the region. The bottom graph (C) shows a NOAA smoke plume analysis for the time of the peak event (indicated by the blue star in the upper graph). The wildfire smoke plumes originated in California; wide regions in the west and midwestern US were similarly impacted.

Supplement A

Preliminary Data LMA Quarter 3, 2020

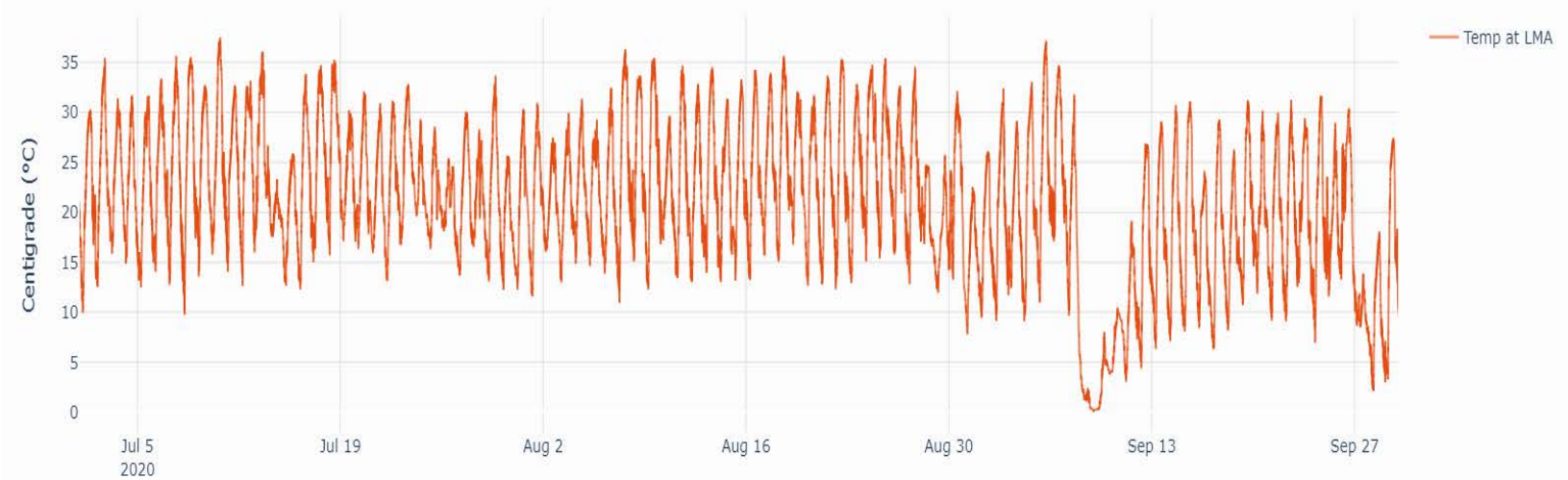

Figure SA1:
LMA temperature record July 1 – September 30, 2020.

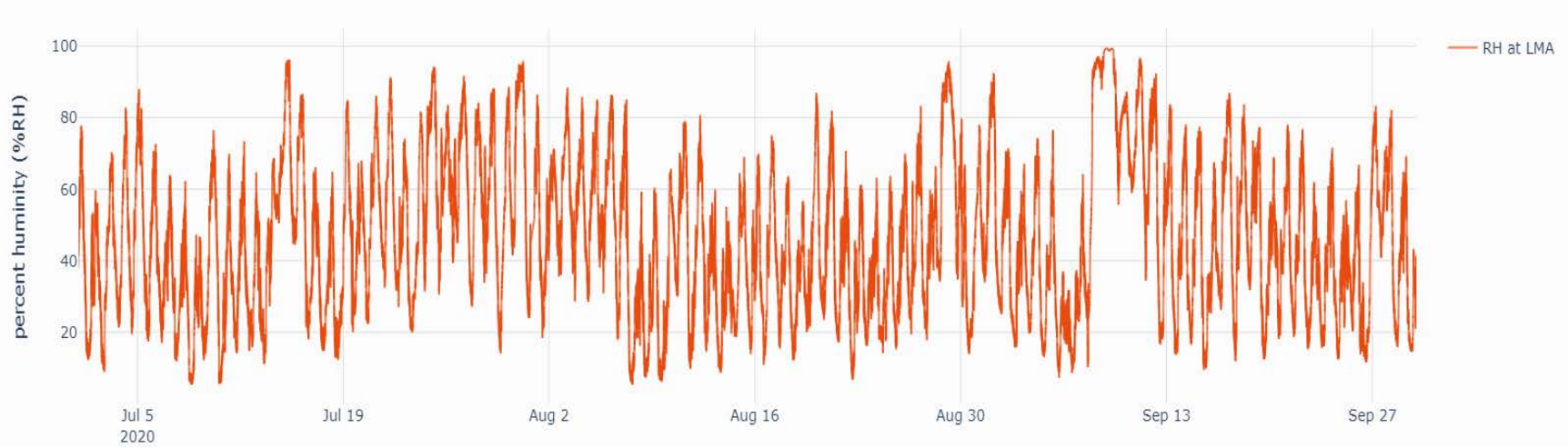

Figure SA2:
LMA relative humidity record July 1 – September 30, 2020.

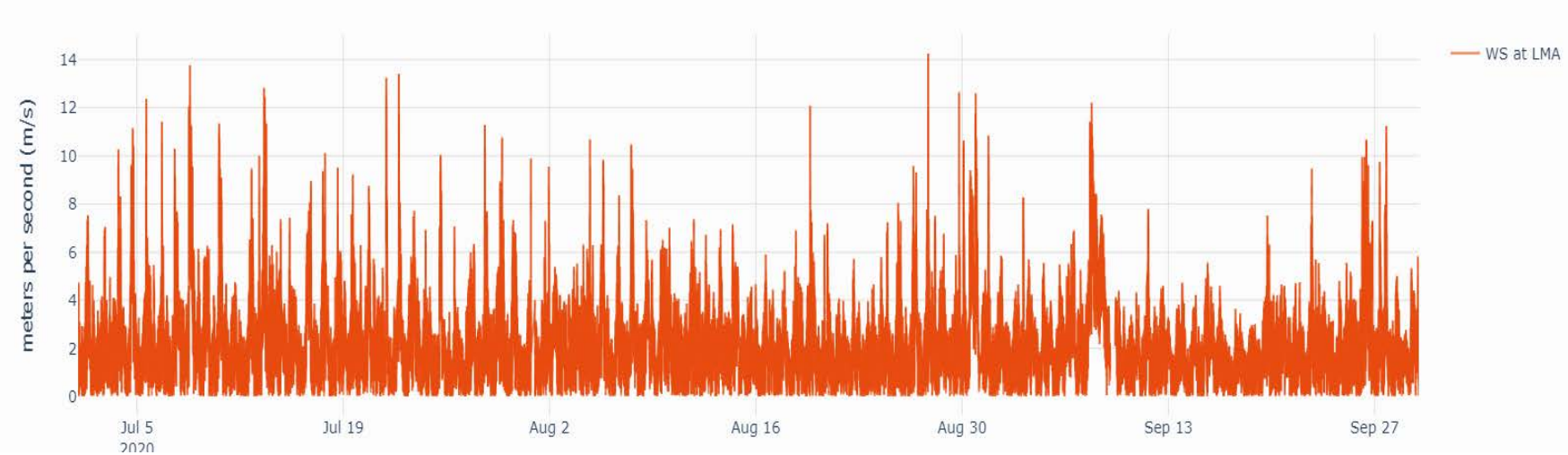

Figure SA3:
LMA wind speed record July 1 – September 30, 2020.

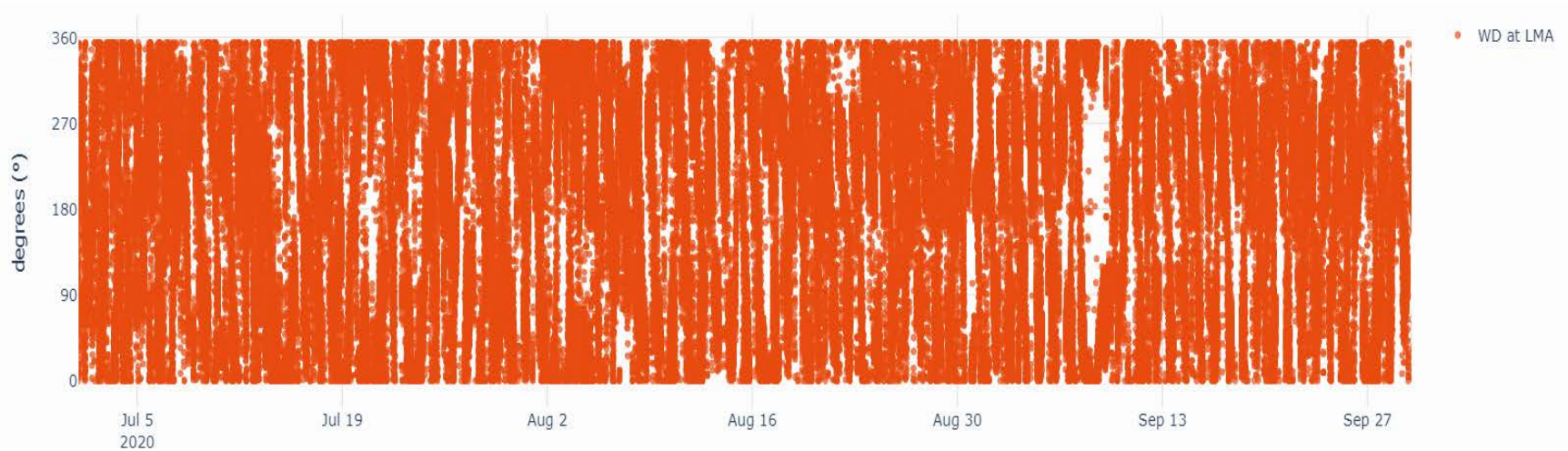

Figure SA4:
LMA wind direction record July 1 – September 30, 2020.

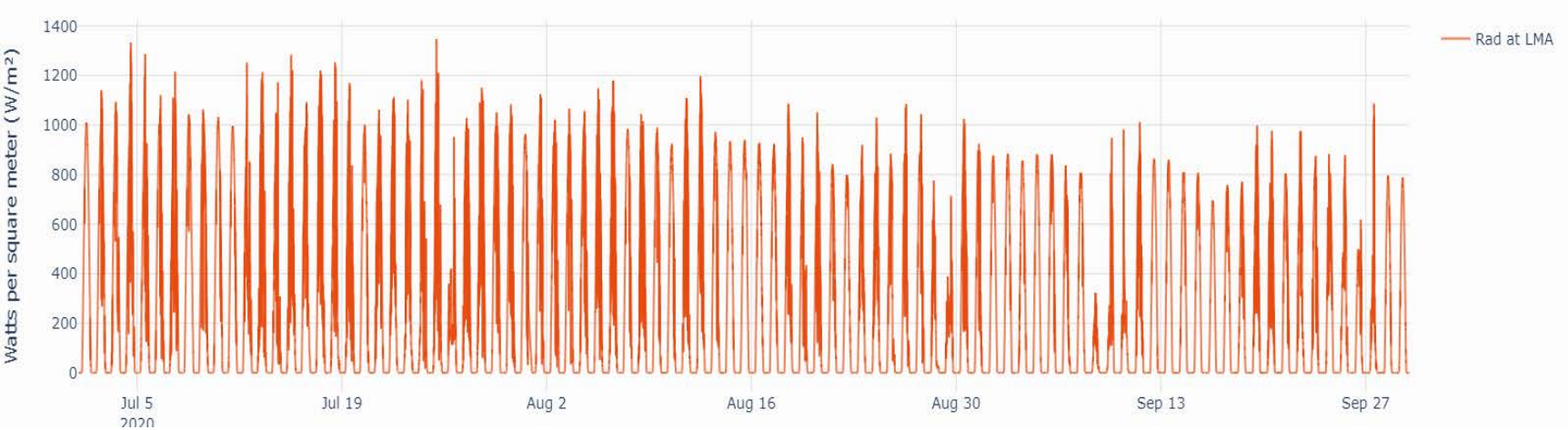

Figure SA5:
LMA solar radiation record July 1 – September 30, 2020.

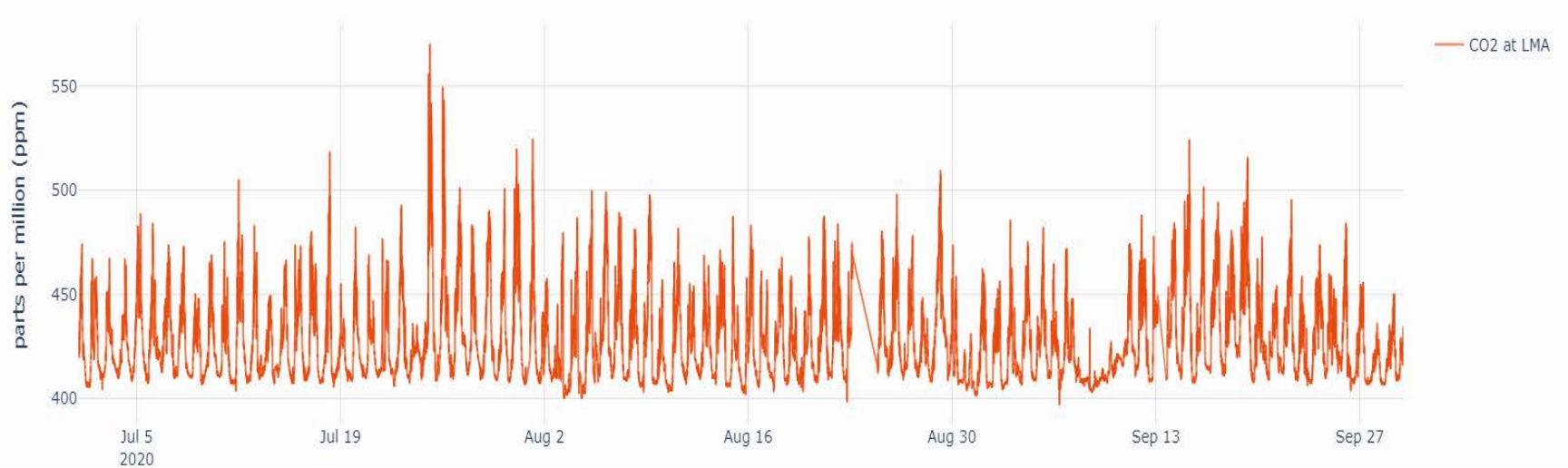

Figure SA6:
LMA CO_2 record January July 1 – September 30, 2020.

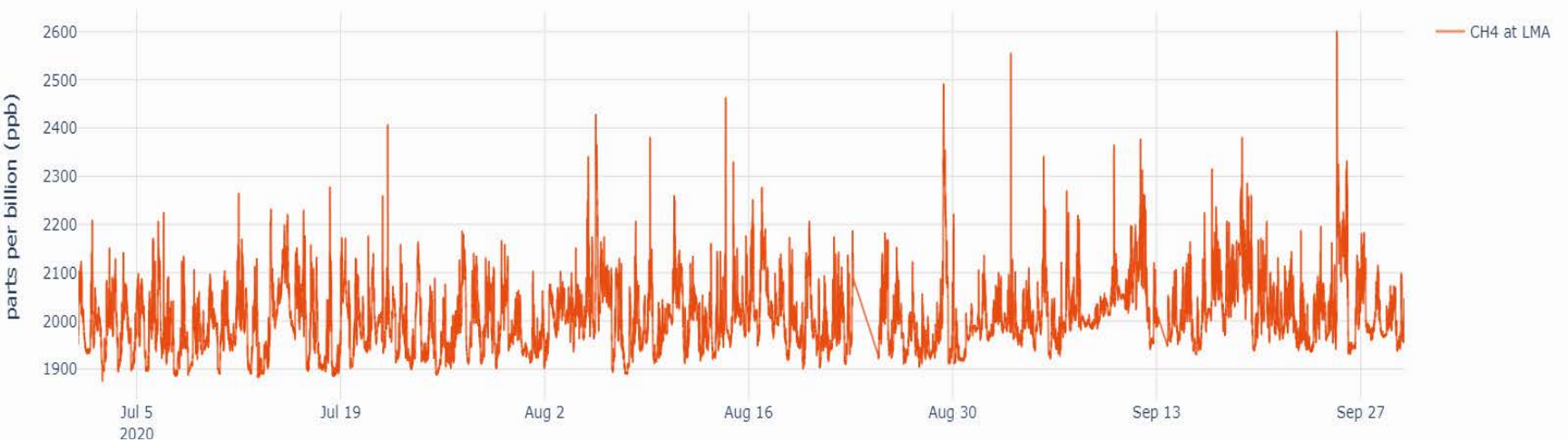

Figure SA7:
LMA CH_4 record January July 1 – September 30, 2020.

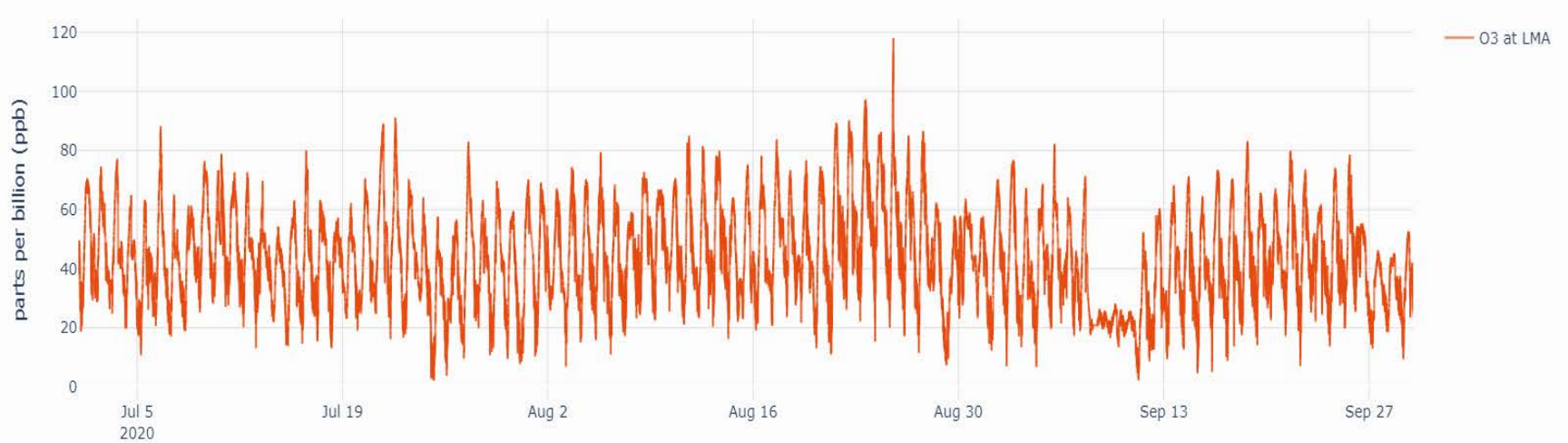

Figure SA8:
LMA ozone record July 1 – September 30, 2020.

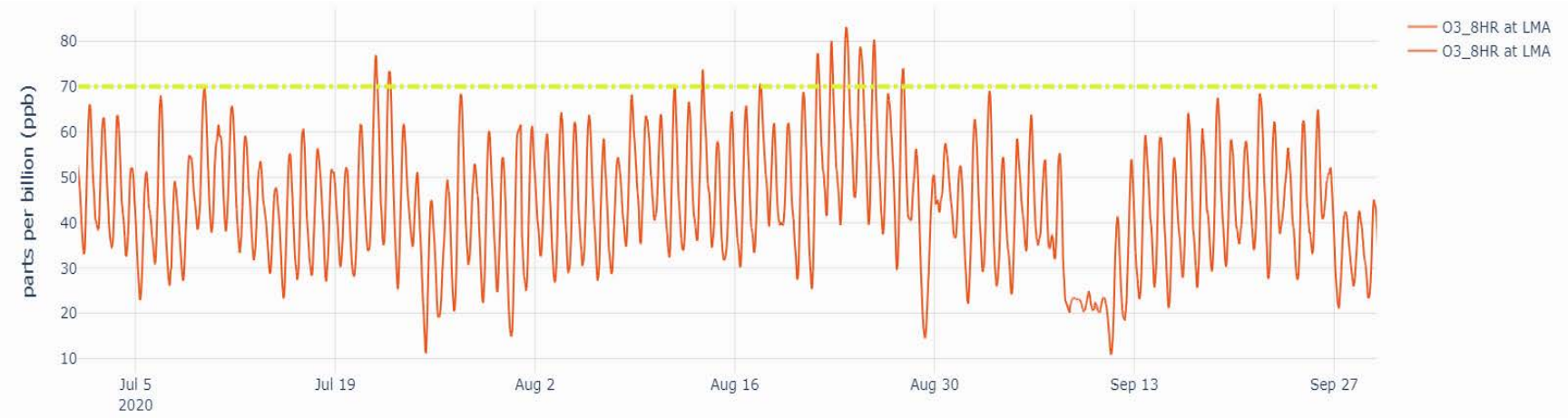

Figure SA9:
LMA ozone 8-hour running average record April 1 – June 30, 2020.

Supplement B

Preliminary Data LUR Quarter 3 2020

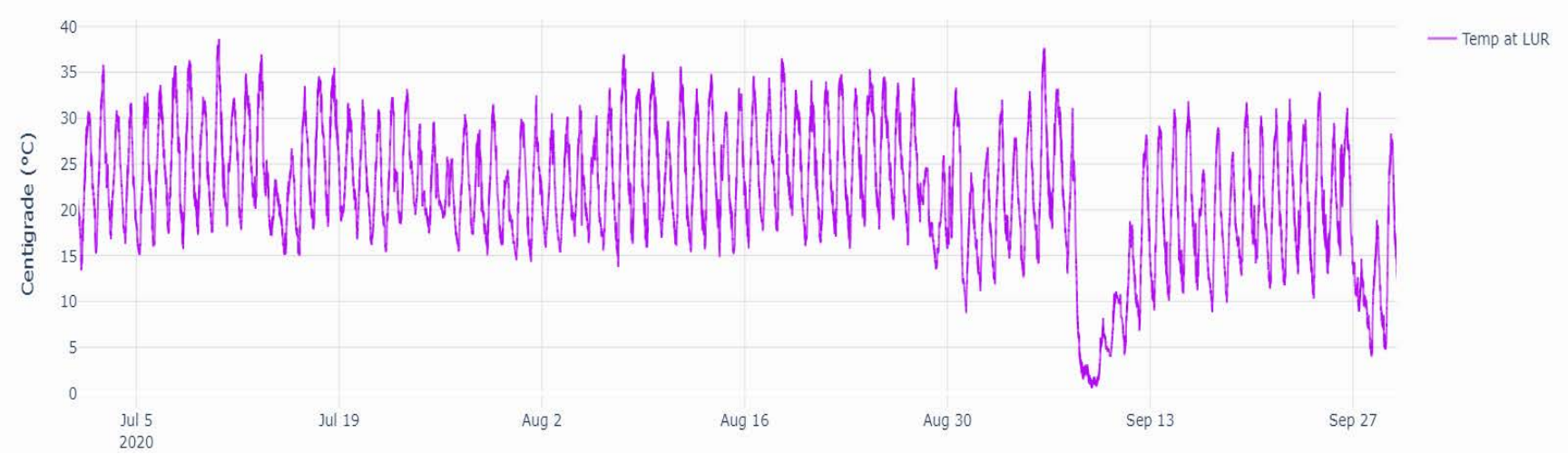

Figure SB1:
LUR temperature record July 1 – September 30, 2020.

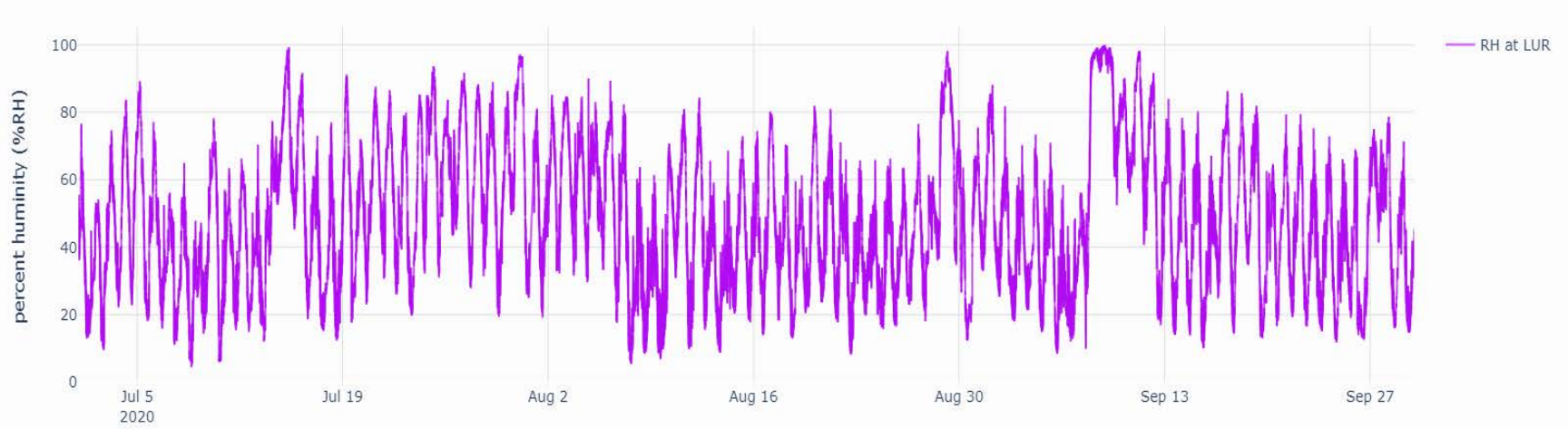

Figure SB2:
LUR relative humidity record July 1 – September 30, 2020.

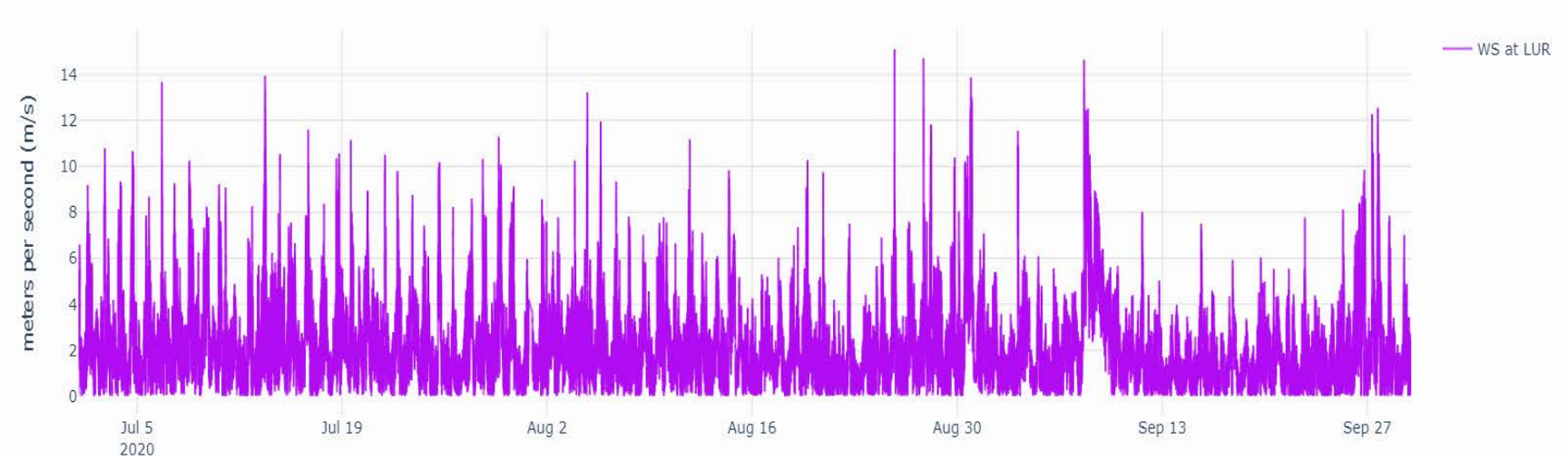

Figure SB3:
LUR wind speed record July 1 – September 30, 2020.

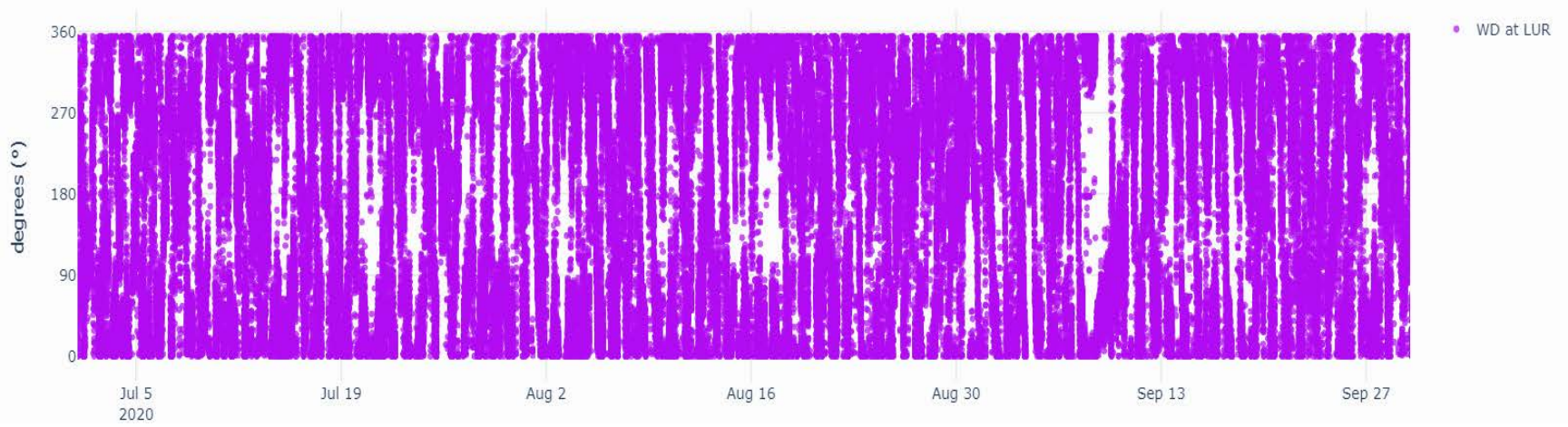

Figure SB4:
LUR wind direction record July 1 – September 30, 2020.

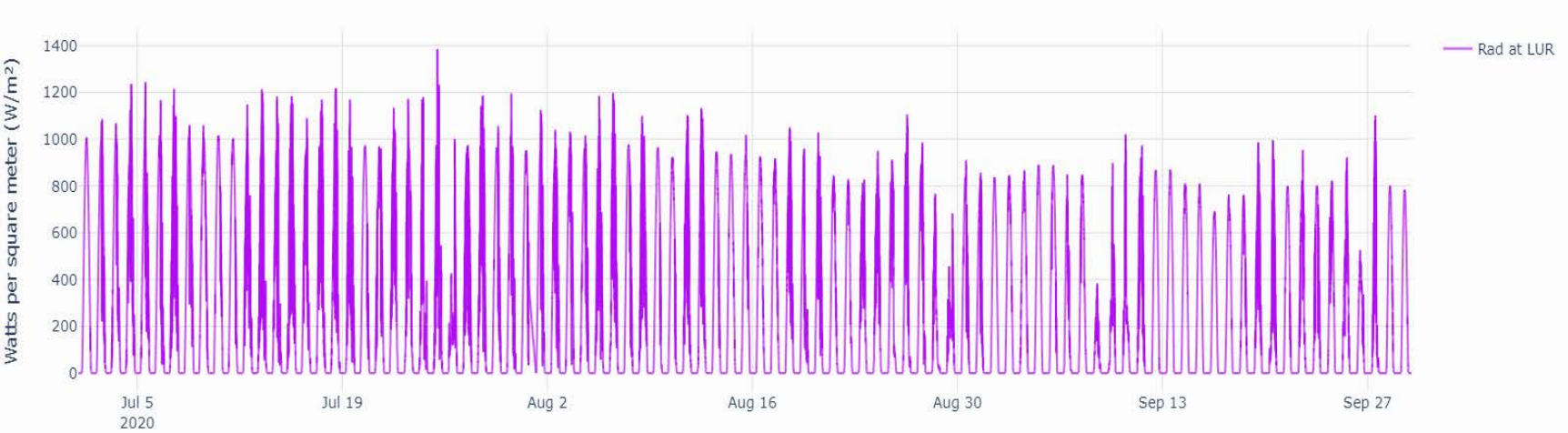

Figure SB5:
LUR solar radiation record July 1 – September 30, 2020.

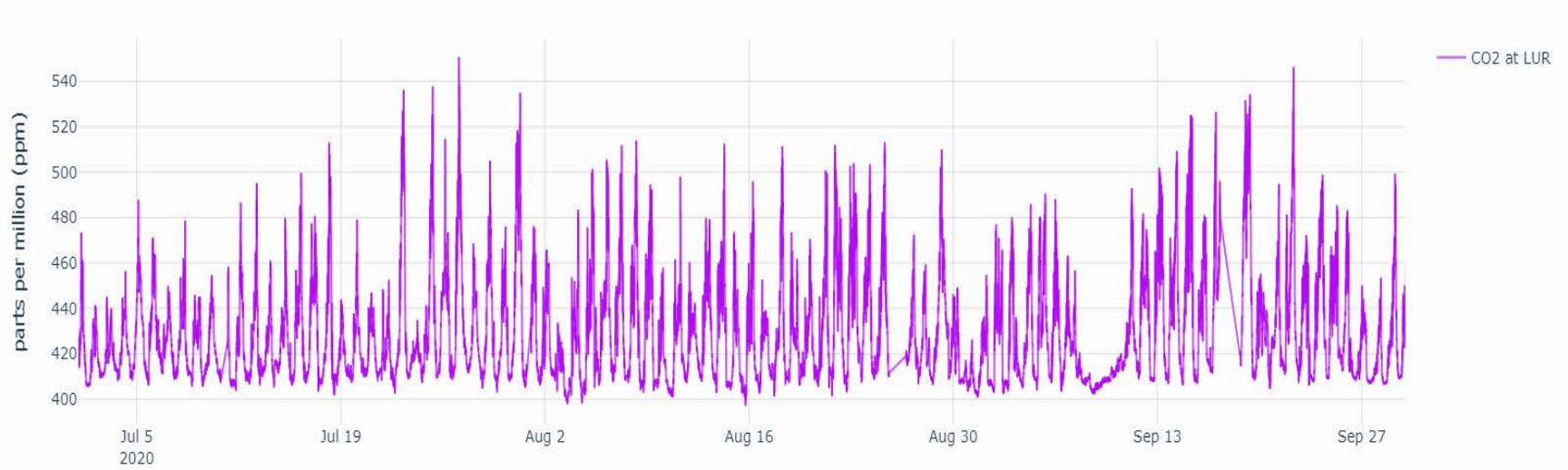

Figure SB6:
LUR CO_2 record July 1 – September 30, 2020.

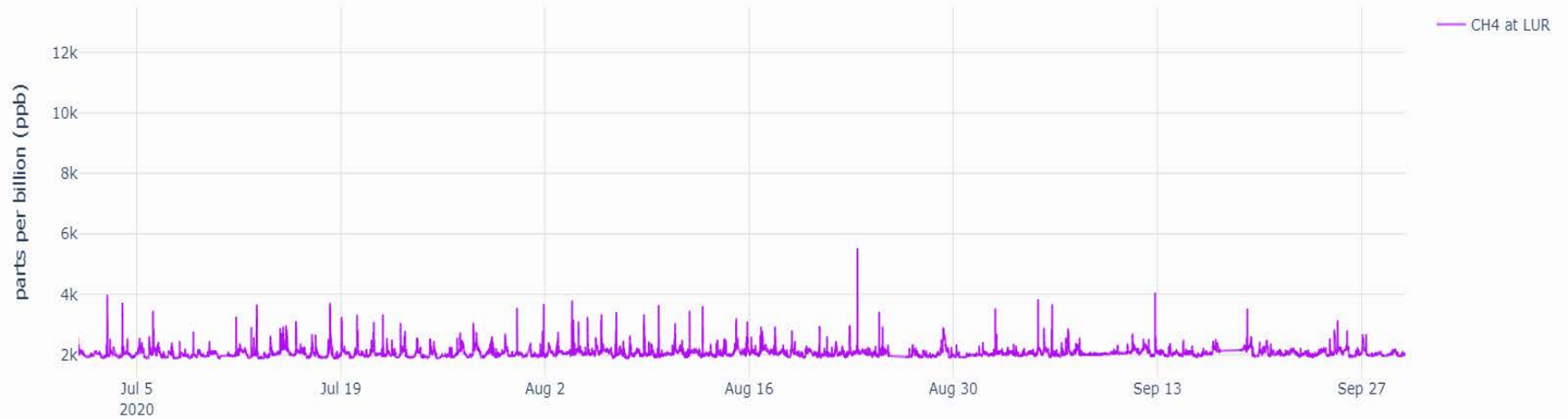

Figure SB7:
LUR methane record July 1 – September 30, 2020.

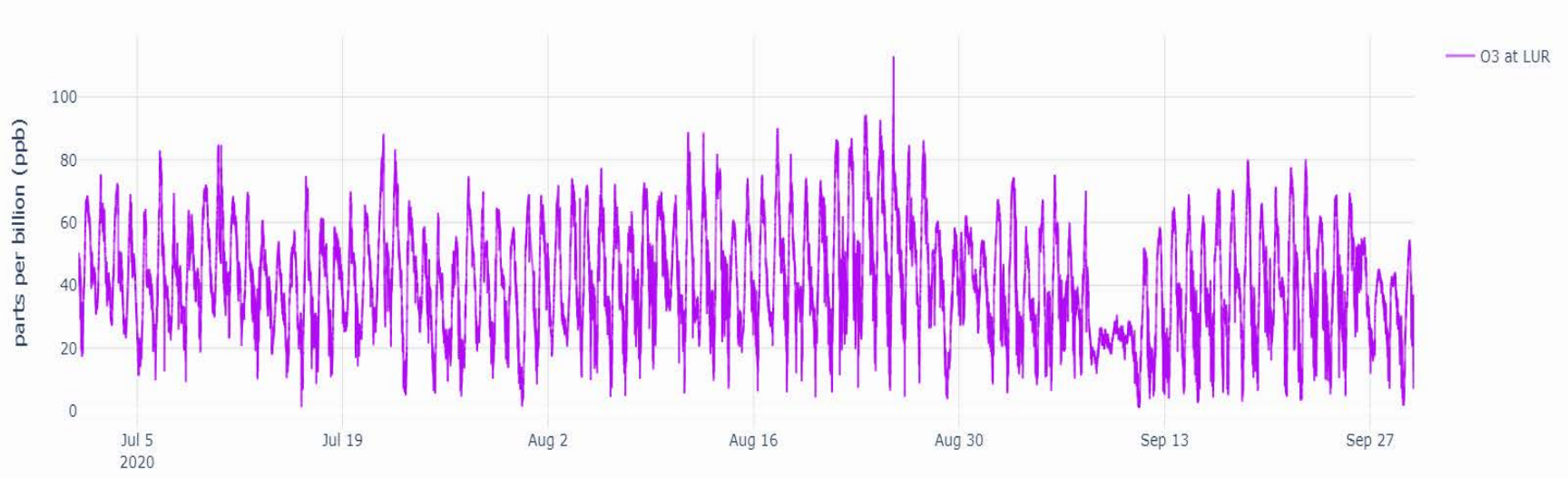

Figure SB8:
LUR ozone record July 1 – September 30, 2020.

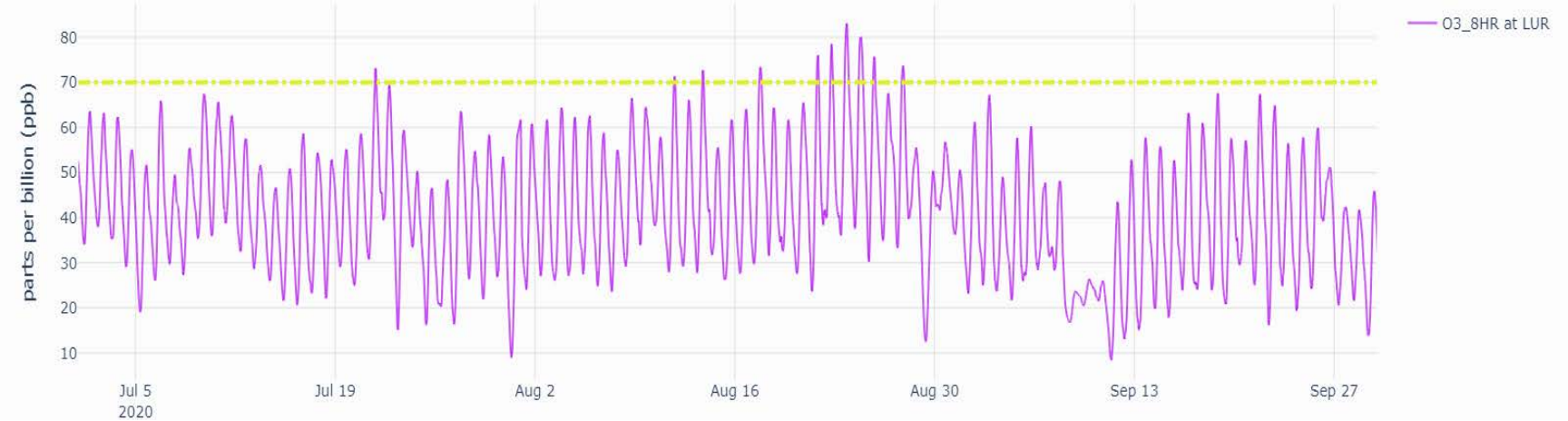

Figure SB9:
LUR ozone 8-hour running average record July 1 – September 30, 2020.

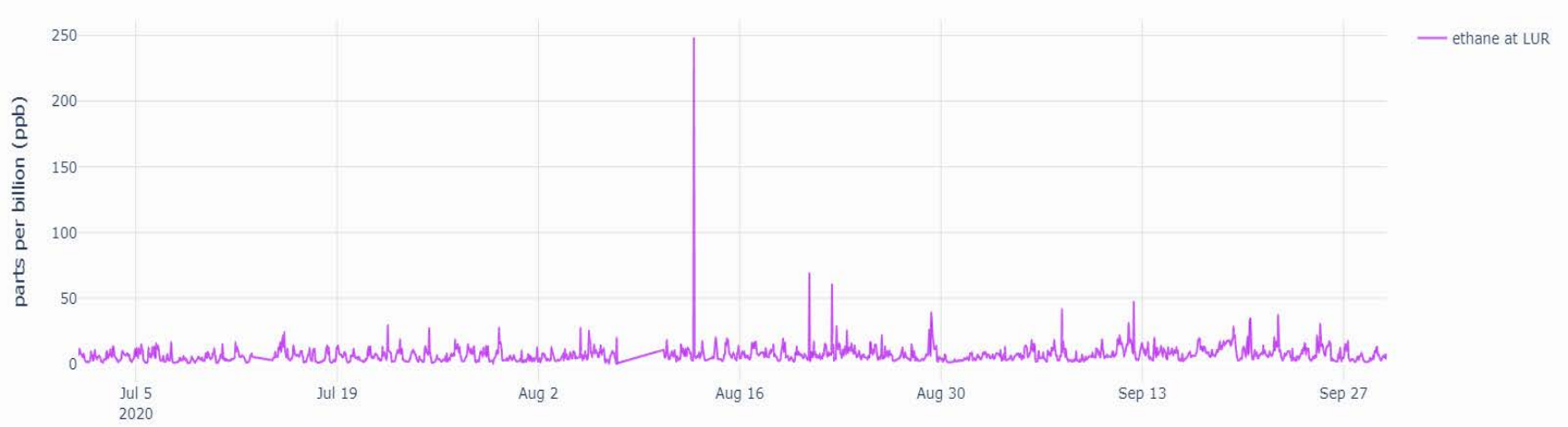

Figure SB10:
LUR ethane record July 1 – September 30, 2020.

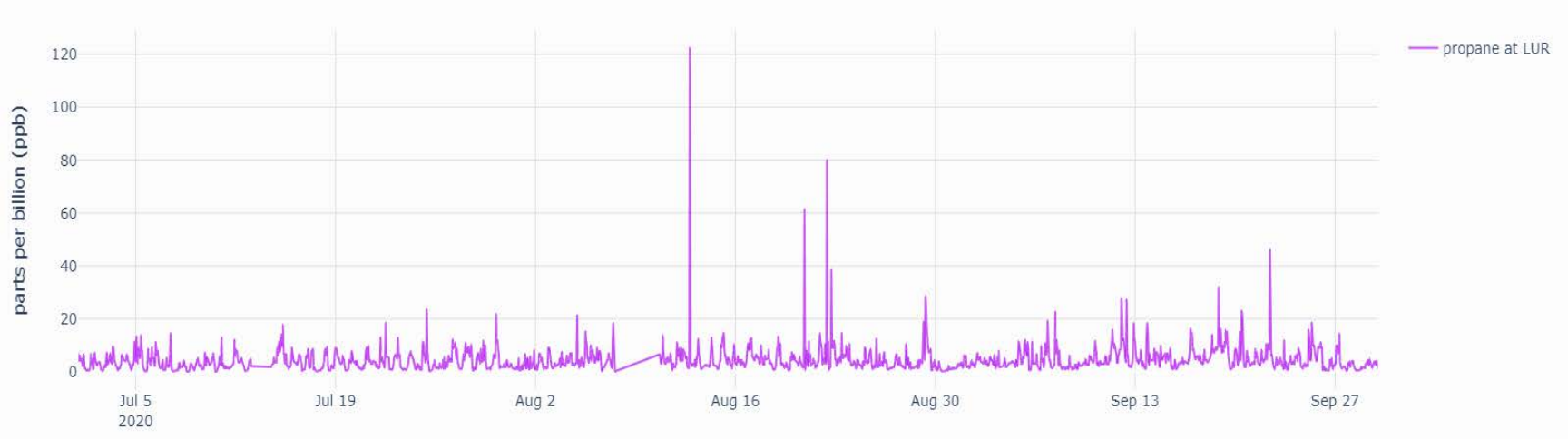

Figure SB11:
LUR propane record July 1 – September 30, 2020.

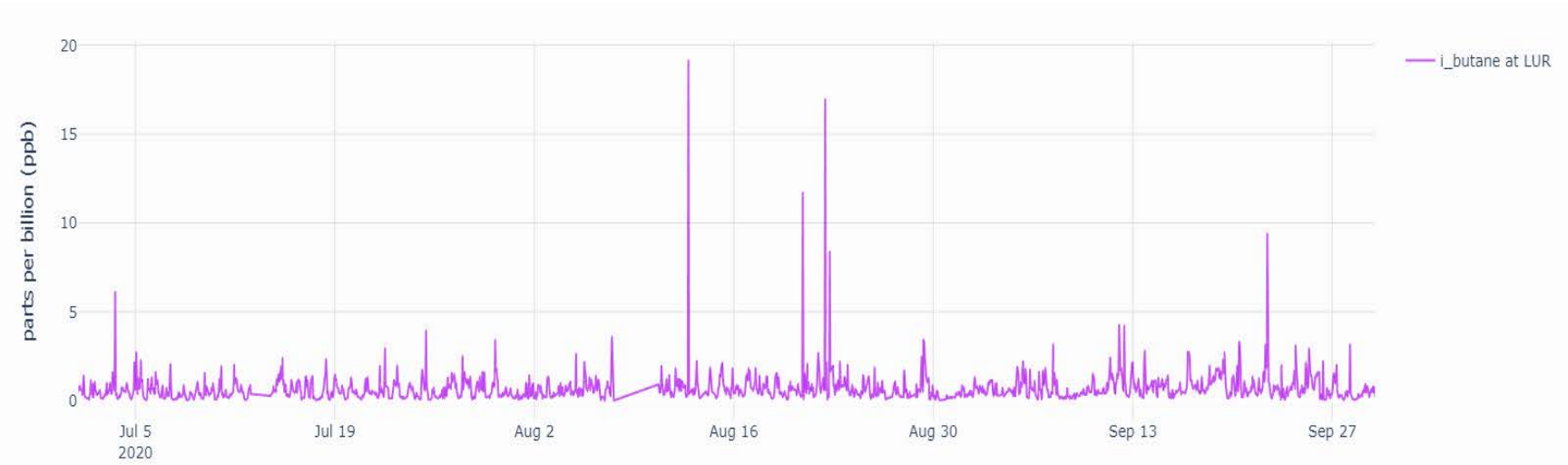

Figure SB12:
LUR i-butane record July 1 – September 30, 2020.

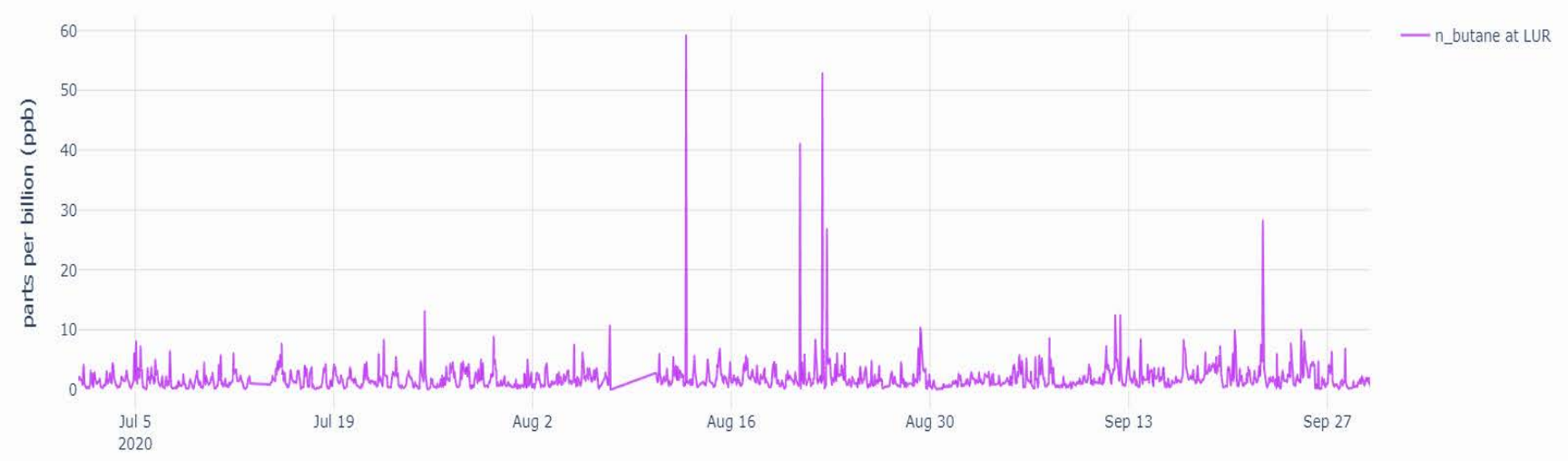

Figure SB13:
LUR n-butane record July 1 – September 30, 2020.

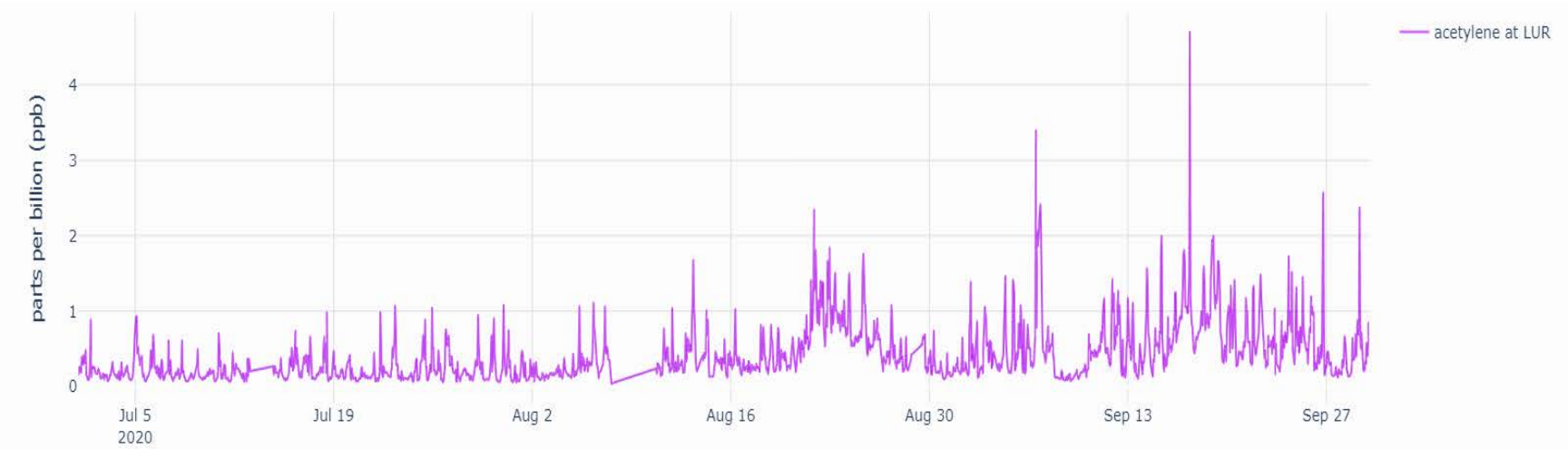

Figure SB14:
LUR acetylene record July 1 – September 30, 2020.

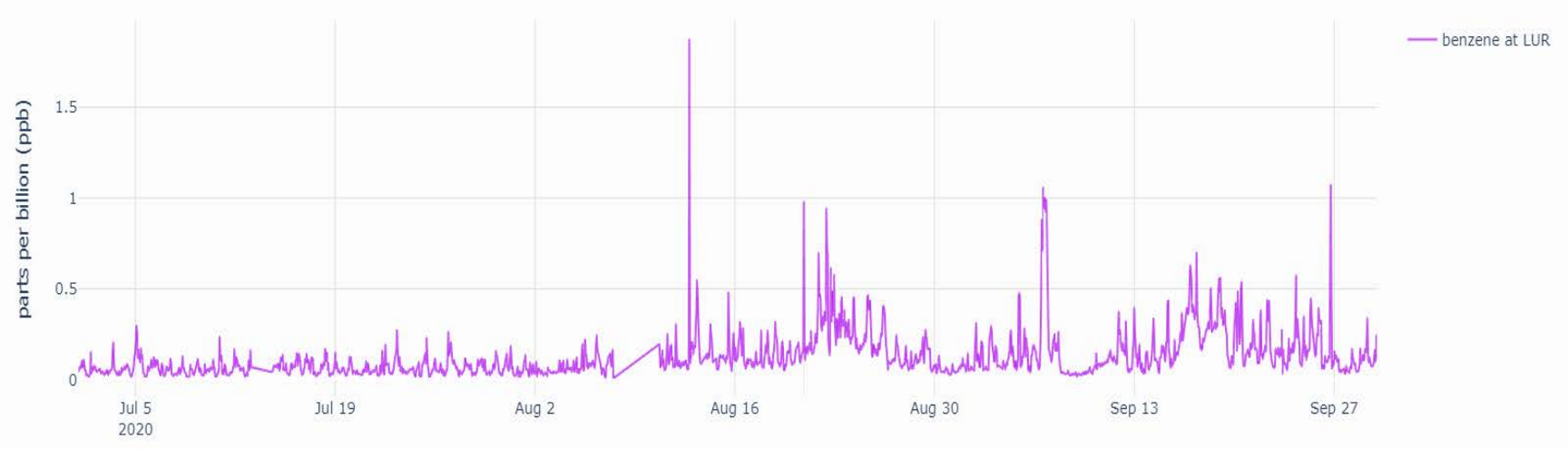

Figure SB15:
LUR benzene record July 1 – September 30, 2020.

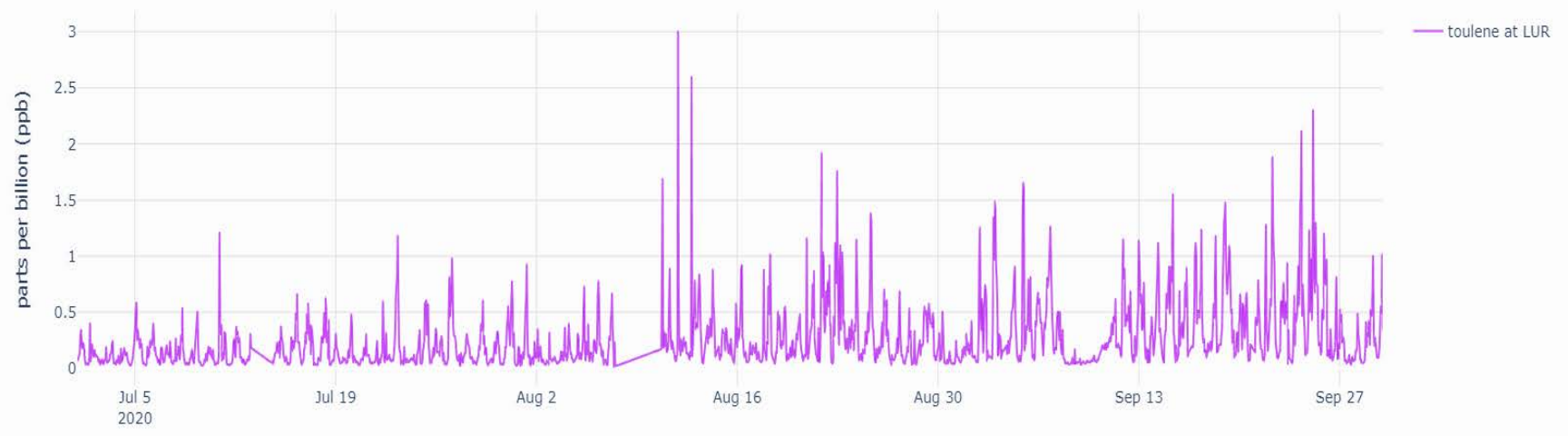

Figure SB16:
LUR toluene record July 1 – September 30, 2020.

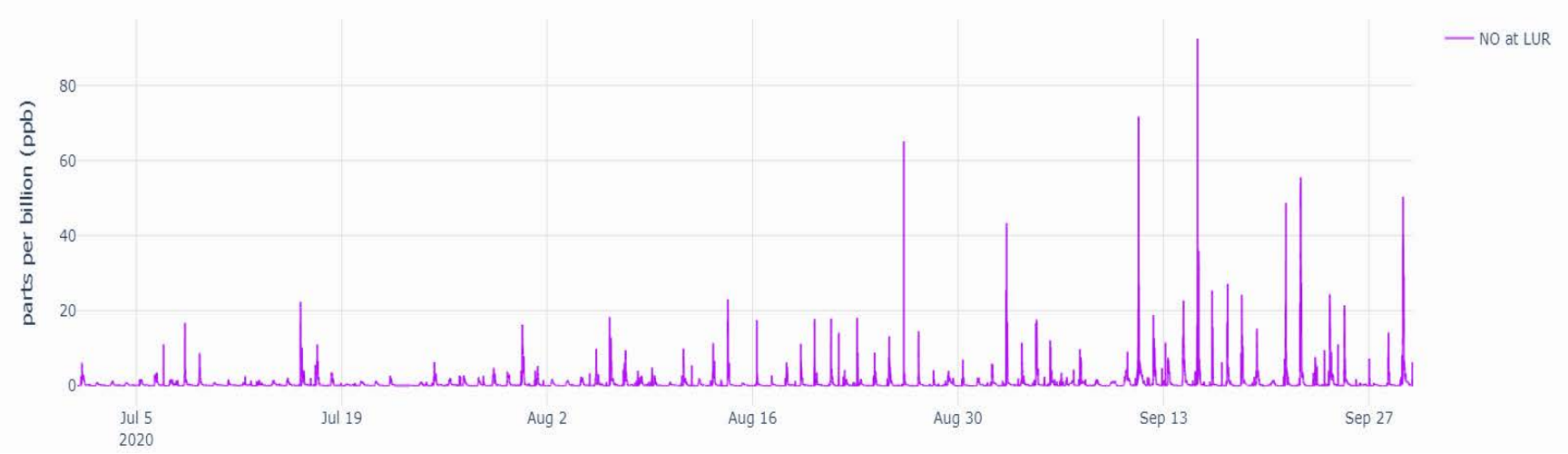

Figure SB17:
LUR nitric oxide record July 1 – September 30, 2020.

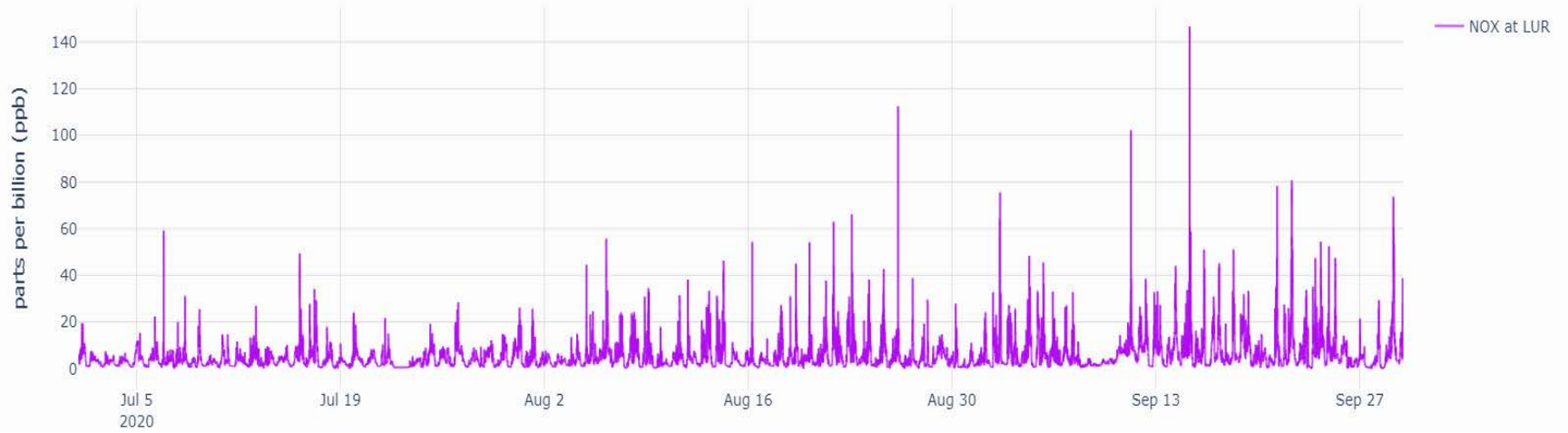

Figure SB18:
LUR nitrogen oxides record July 1 – September 30, 2020.

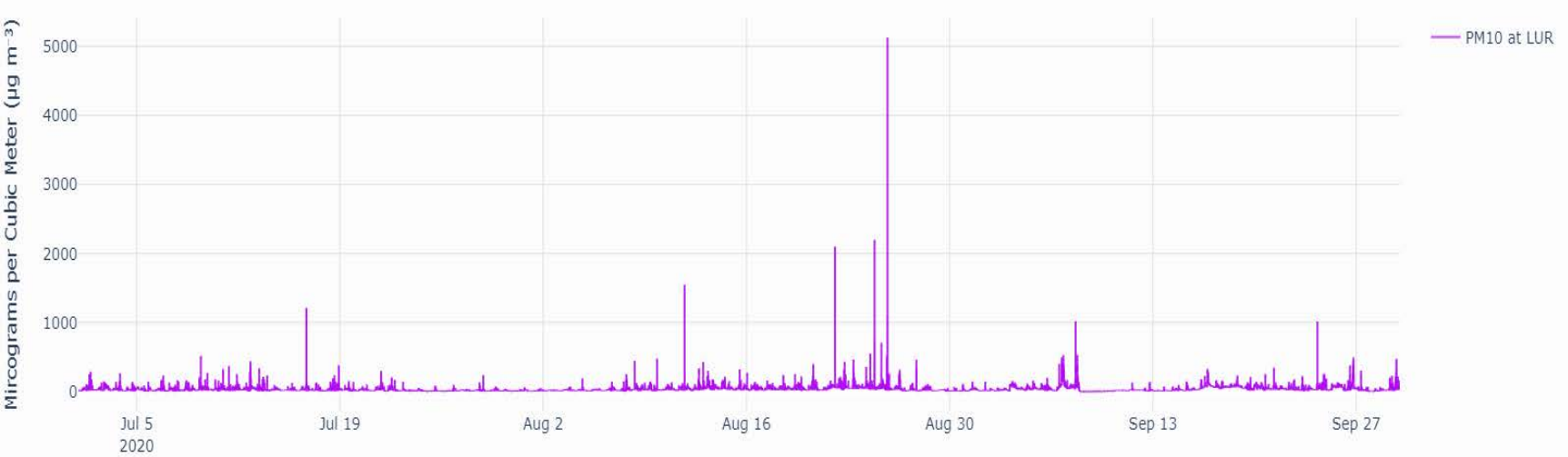

Figure SB19:
LUR coarse particulate matter PM_{10} record for July 1 – September 30, 2020.

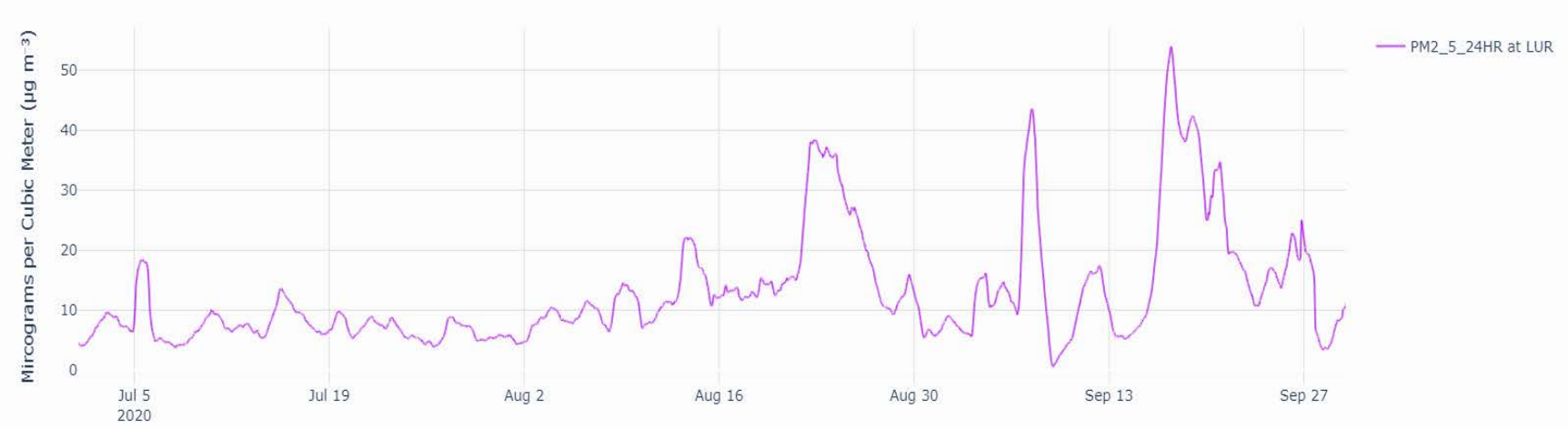

Figure SB20:
LUR fine particulate matter $PM_{2.5}$ record for July 1 – September 30, 2020.

Supplement C

Comparison of Preliminary Data LMA & LUR 2020

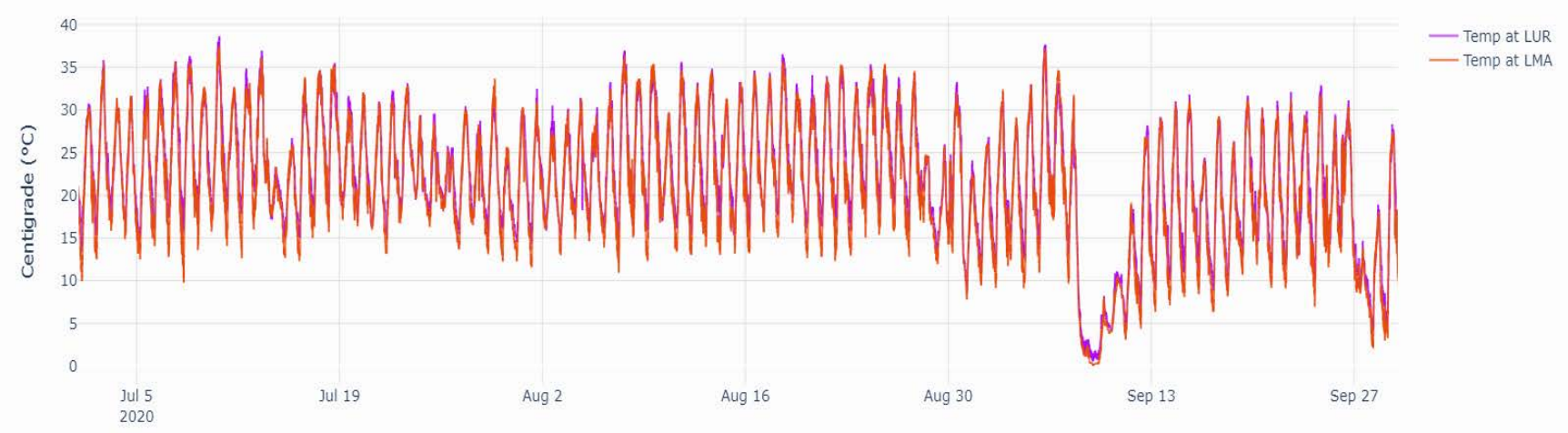

Figure SC1:
LMA & LUR Temperature record July 1 – September 30, 2020.

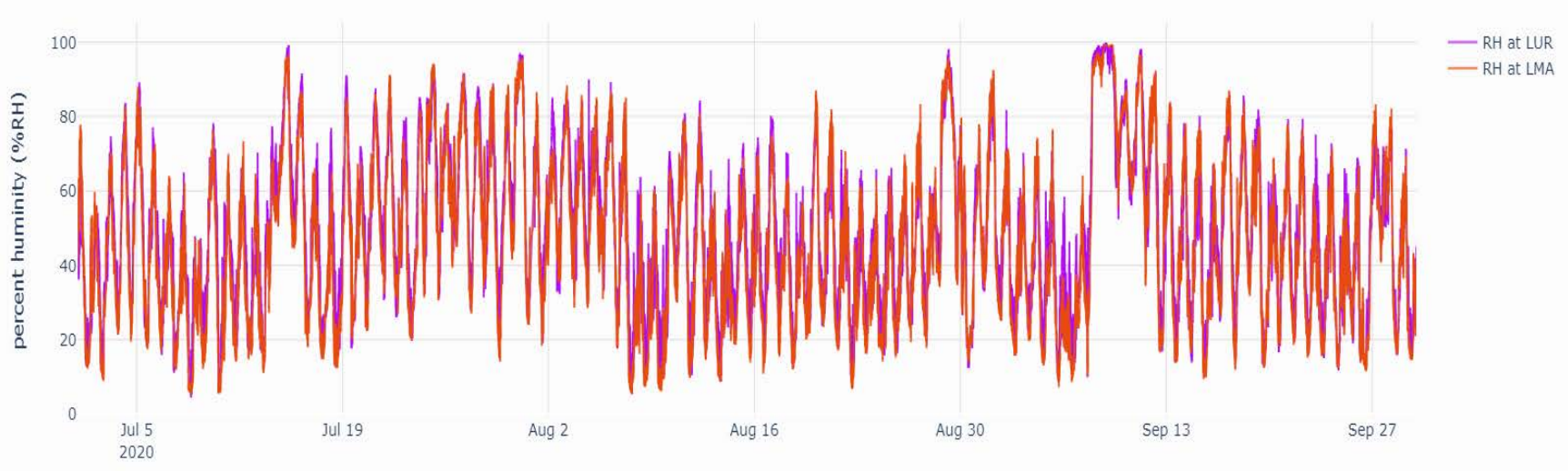

Figure SC2:
LMA & LUR relative humidity record September July 1 – September 30, 2020.

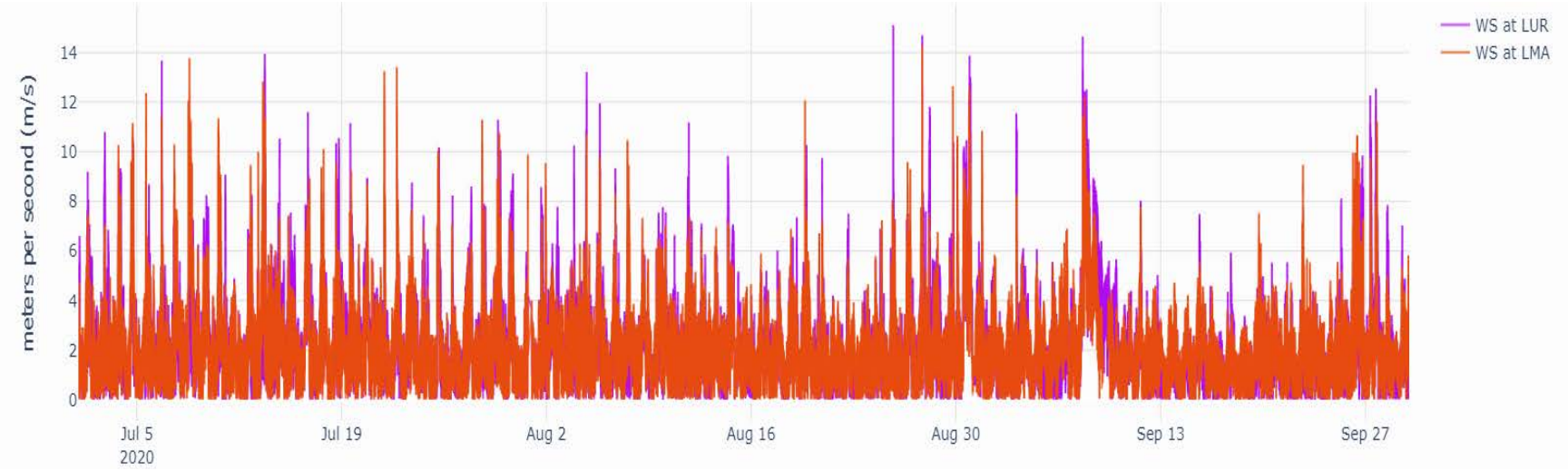

Figure SC3:
LMA & LUR wind speed record July 1 – September 30, 2020.

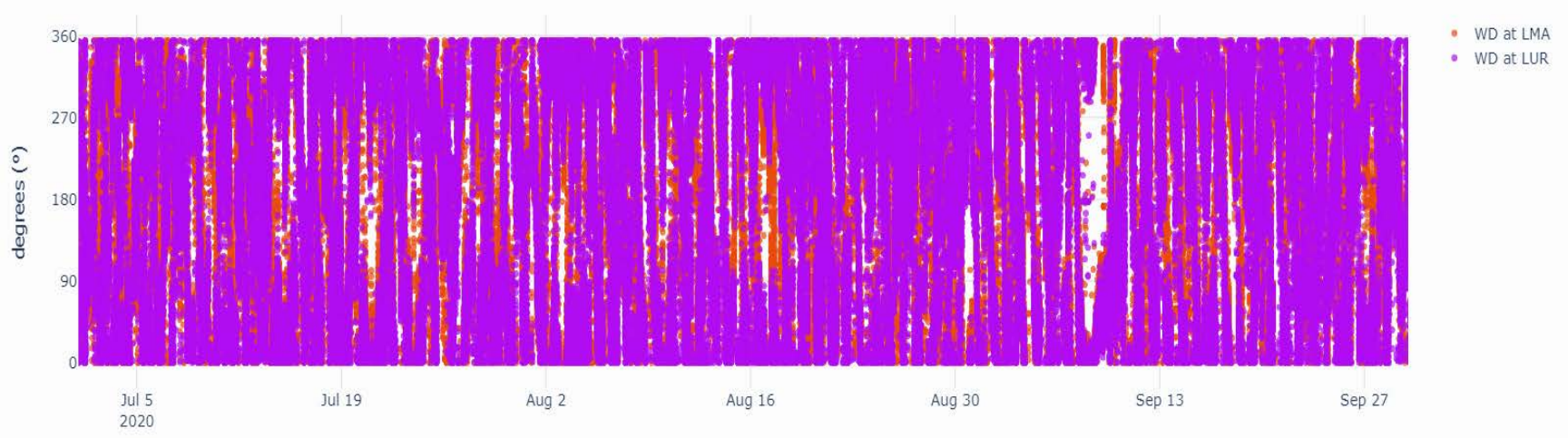

Figure SC4:
LMA & LUR wind direction record July 1 – September 30, 2020.

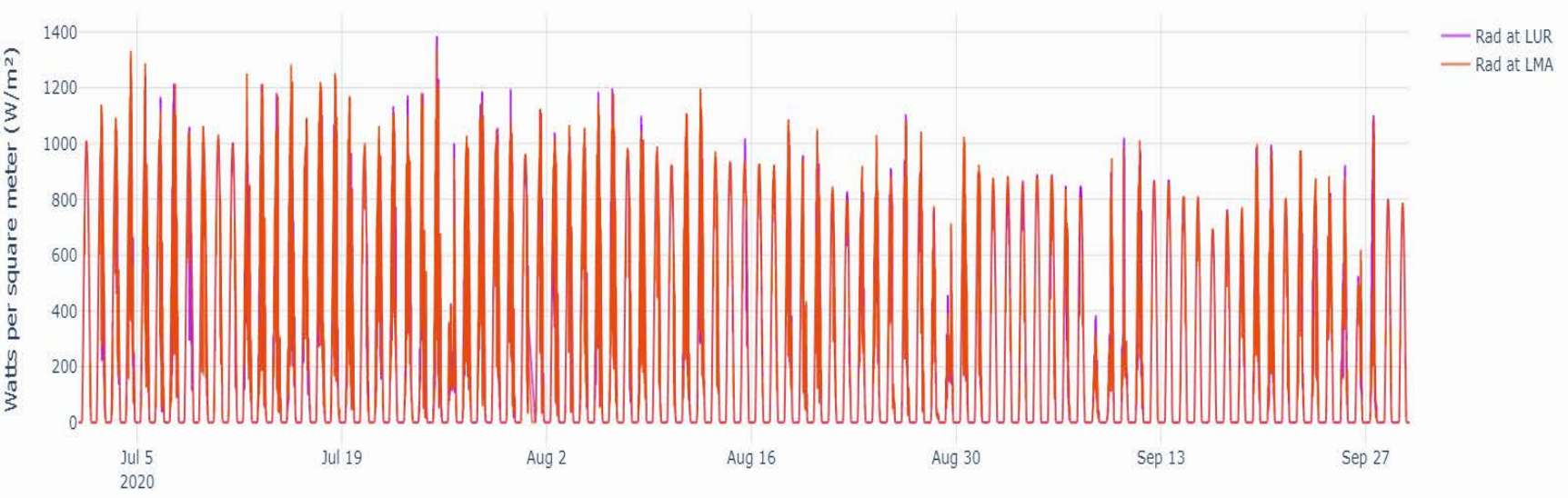

Figure SC5:
LMA & LUR solar radiation record September July 1 – September 30, 2020.

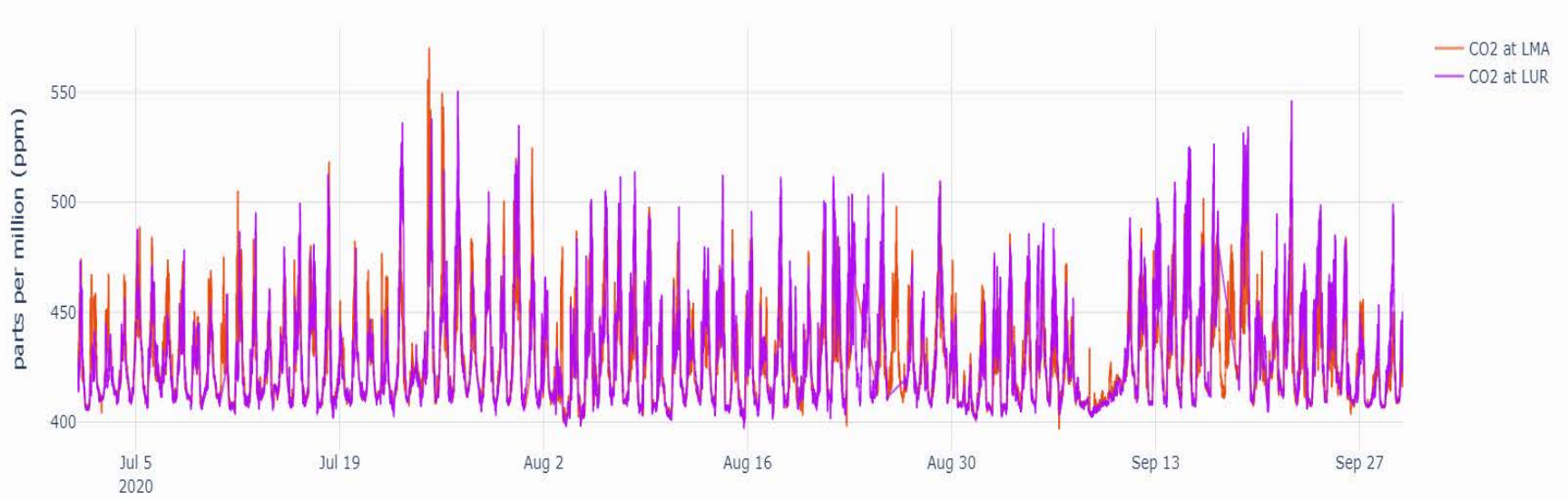

Figure SC6:
LMA & LUR CO_2 record September July 1 – September 30, 2020.

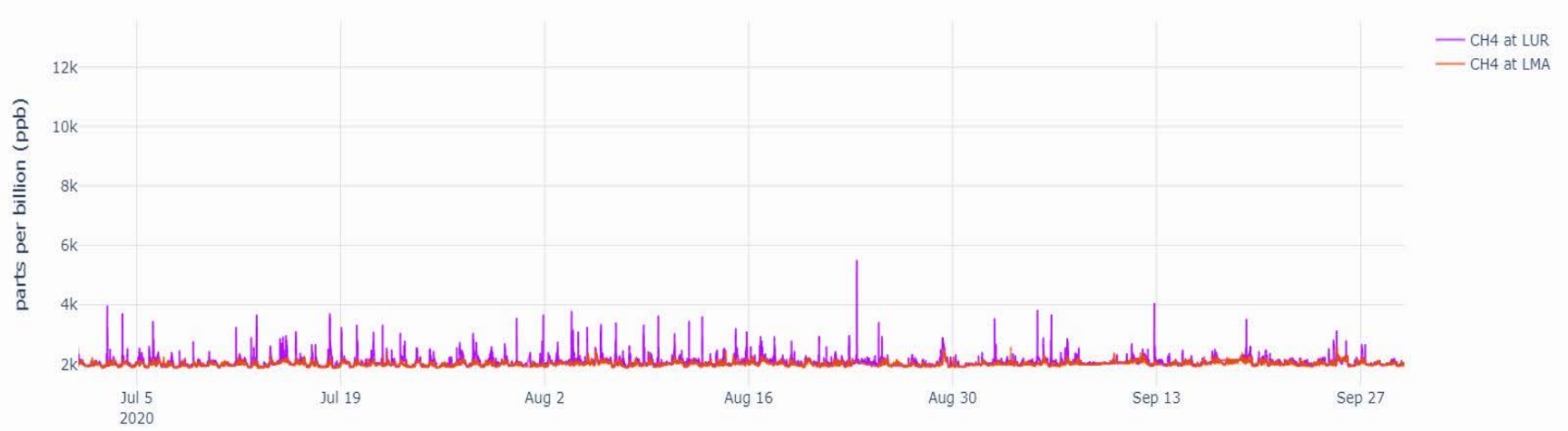

Figure SC7:
LMA & LUR methane record September July 1 – September 30, 2020.

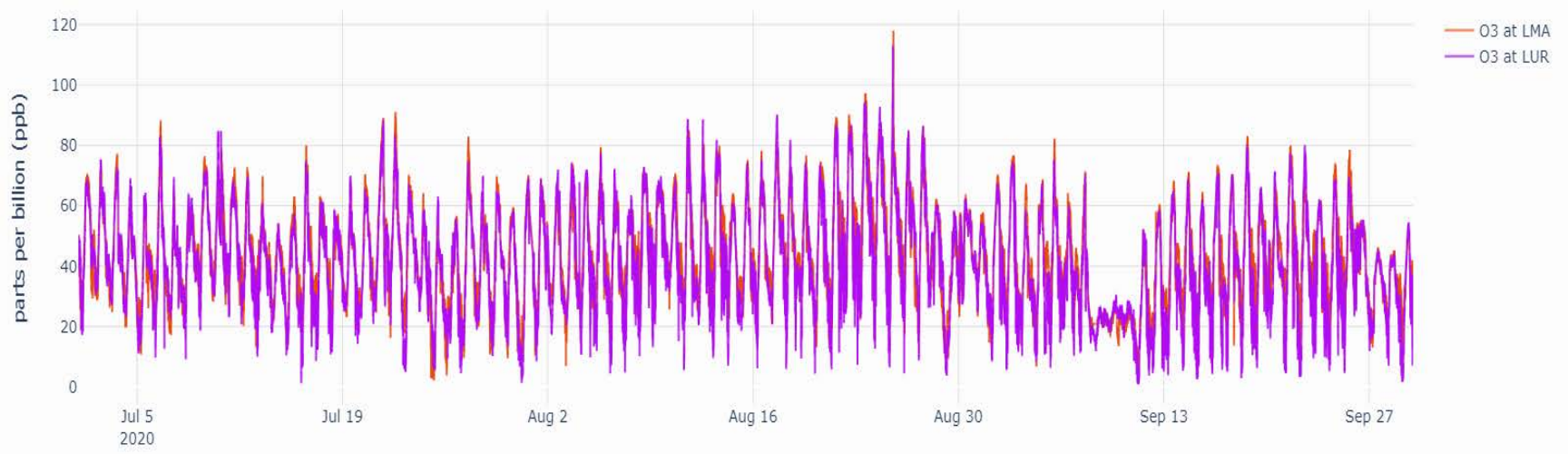

Figure SC8:
LMA & LUR ozone record September July 1 – September 30, 2020.

Supplement D

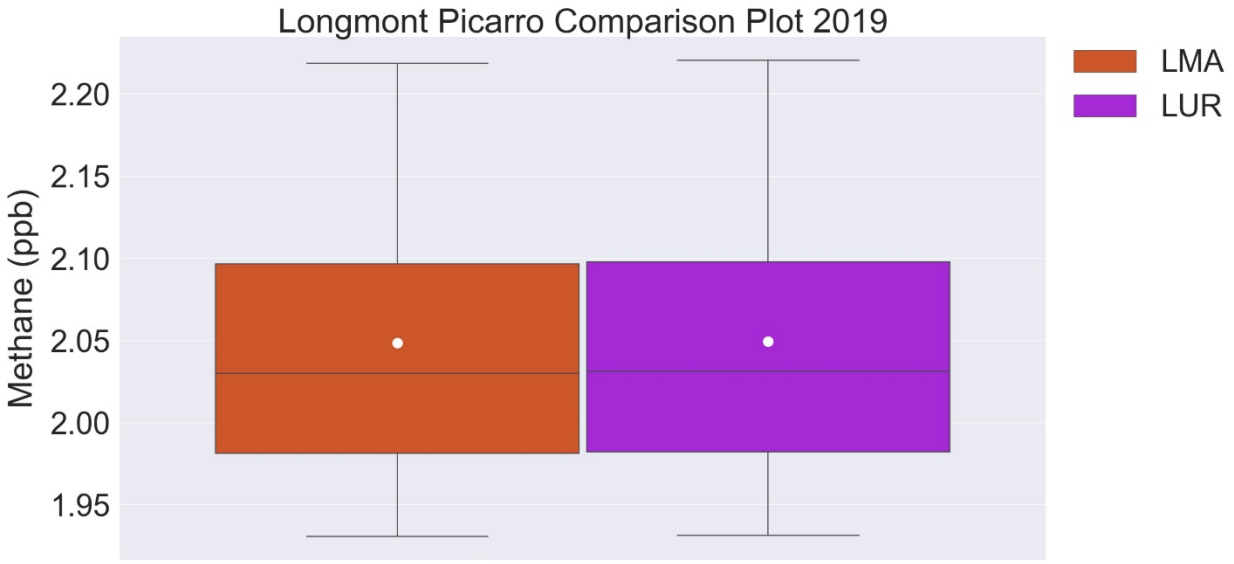

Figure SD1:
Box-whisker plot statistical analysis of monitoring results from two Picarro methane/CO_2 analyzers while they were operated side-by-side, sampling the same air, at LMA during September – December 2019.

Table SD1:
Results for percentile values from each of the two monitors while they were operated side-by-side at LMA. The 'LUR' labeled analyzer is the unit that was subsequently moved to LUR on December 13. Data are in units of ppm.

Stats	LMA	LUR
mean	2.048	2.049
std	0.096	0.096
min	1.910	1.910
5%	1.931	1.931
25%	1.981	1.982
50%	2.030	2.031
75%	2.096	2.098
95%	2.219	2.220
max	3.019	3.021

Supplement E

Comparison of Nitric Oxides Measurement Results from Side-by-Side Operation of a Thermo Scientific Instruments 42iQ and a Teledyne T200UP Analyzer Sampling Ambient Air at LUR

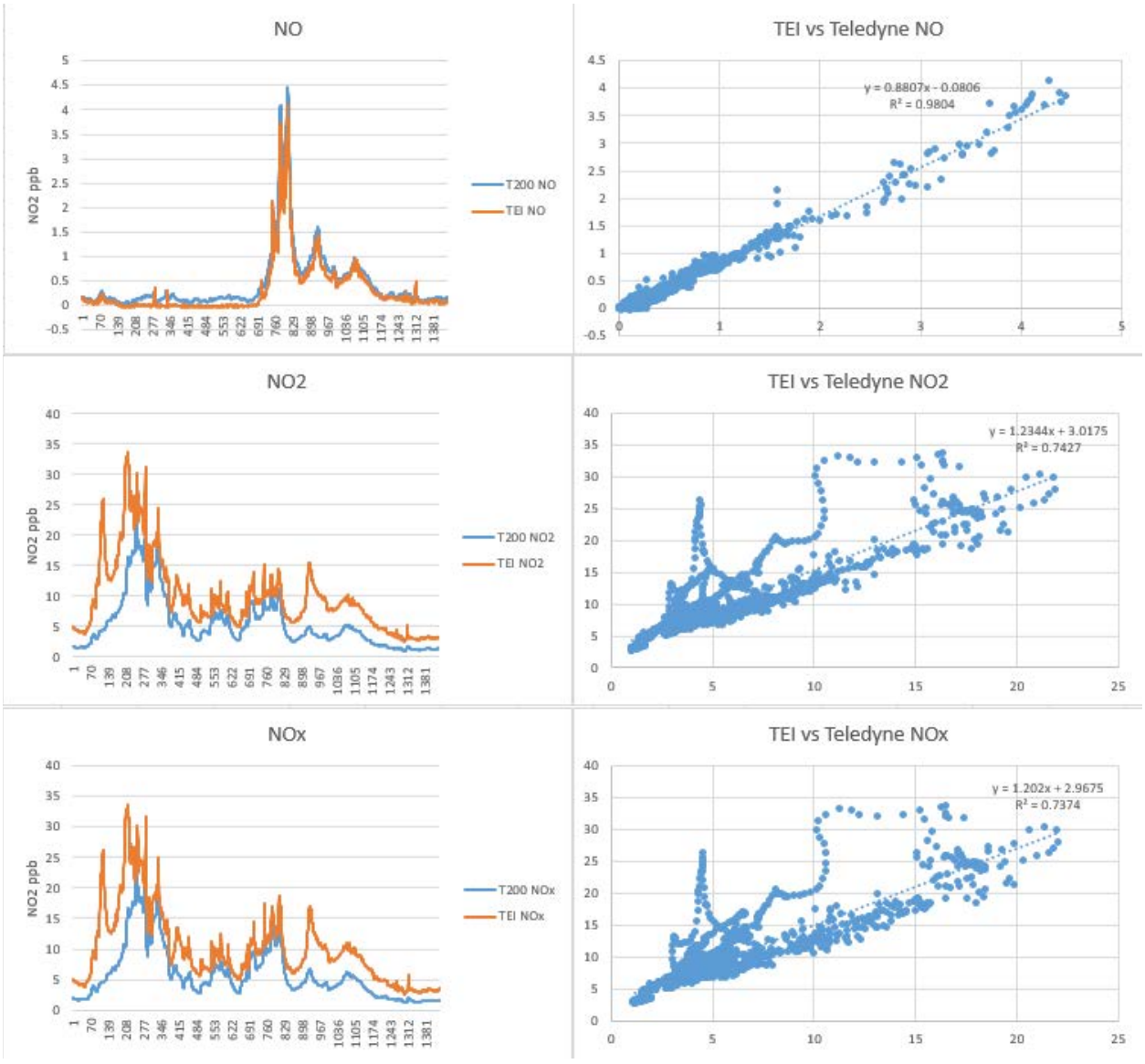

Figure SE1:
Monitoring results for nitric oxide (NO), nitrogen dioxide (NO_2), and NO_x (NO + NO_2) from the side-by-side operation of both analyzers at LUR on June 12, 2020. The graphs on the left show the time series results over the 24-hour time interval (x-axis scale is in minutes after midnight). Graphs on the right show the linear regression results with the data from the Thermo Scientific (TEI) analyzer (y-axis) plotted against the Teledyne analyzers (x-axis). The linear regression results from the comparison are added to the graphs.

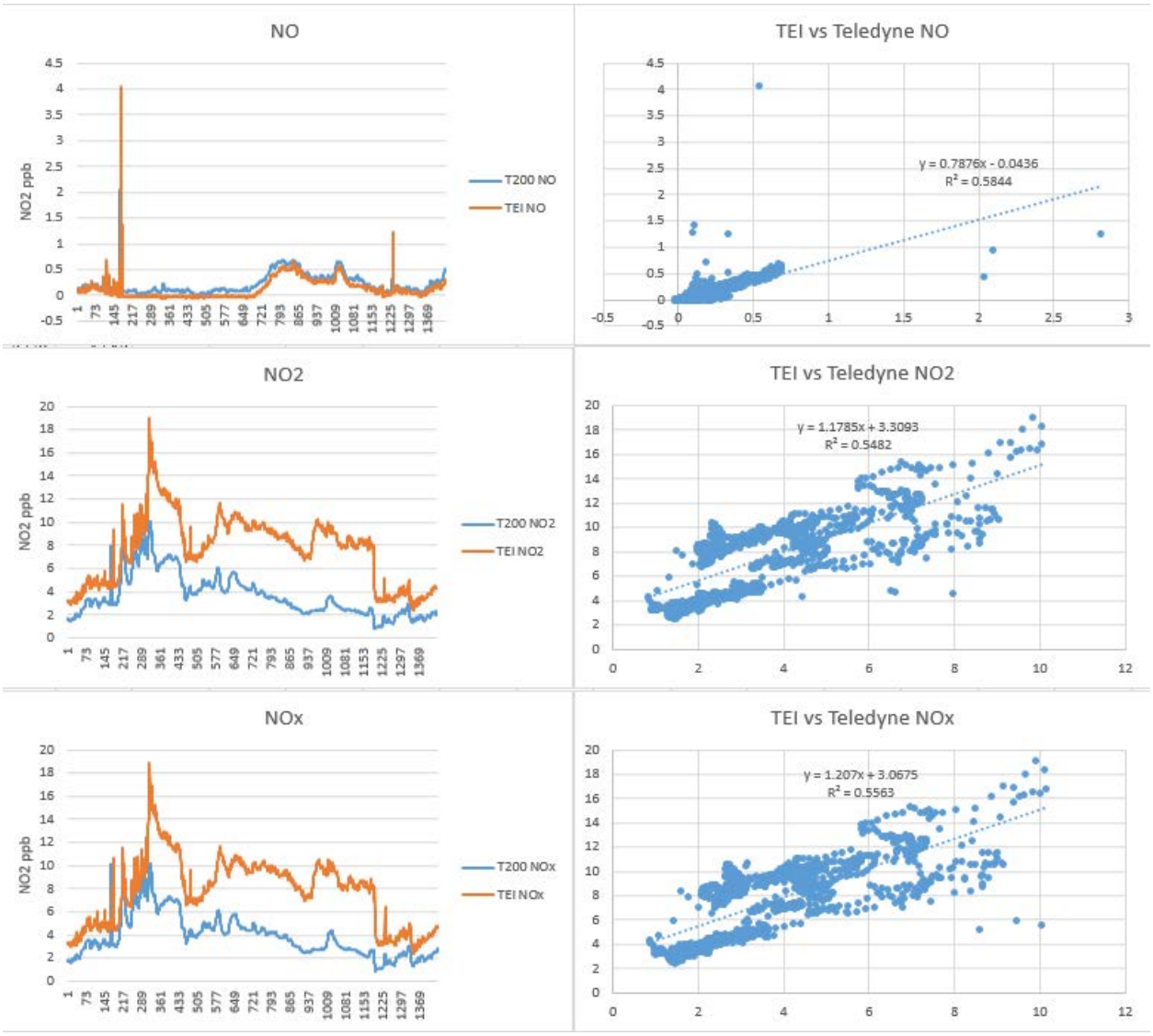

Figure SE2:
Monitoring results for nitric oxide (NO), nitrogen dioxide (NO_2), and NO_x ($NO + NO_2$) from the side-by-side operation of both analyzers at LUR on June 13, 2020. The graphs on the left show the time series results over the 24-hour time interval (x-axis scale is in minutes after midnight). Graphs on the right show the linear regression results with the data from the Thermo Scientific (TEI) analyzer (y-axis) plotted against the Teledyne analyzers (x-axis). The linear regression results from the comparison are added to the graphs.

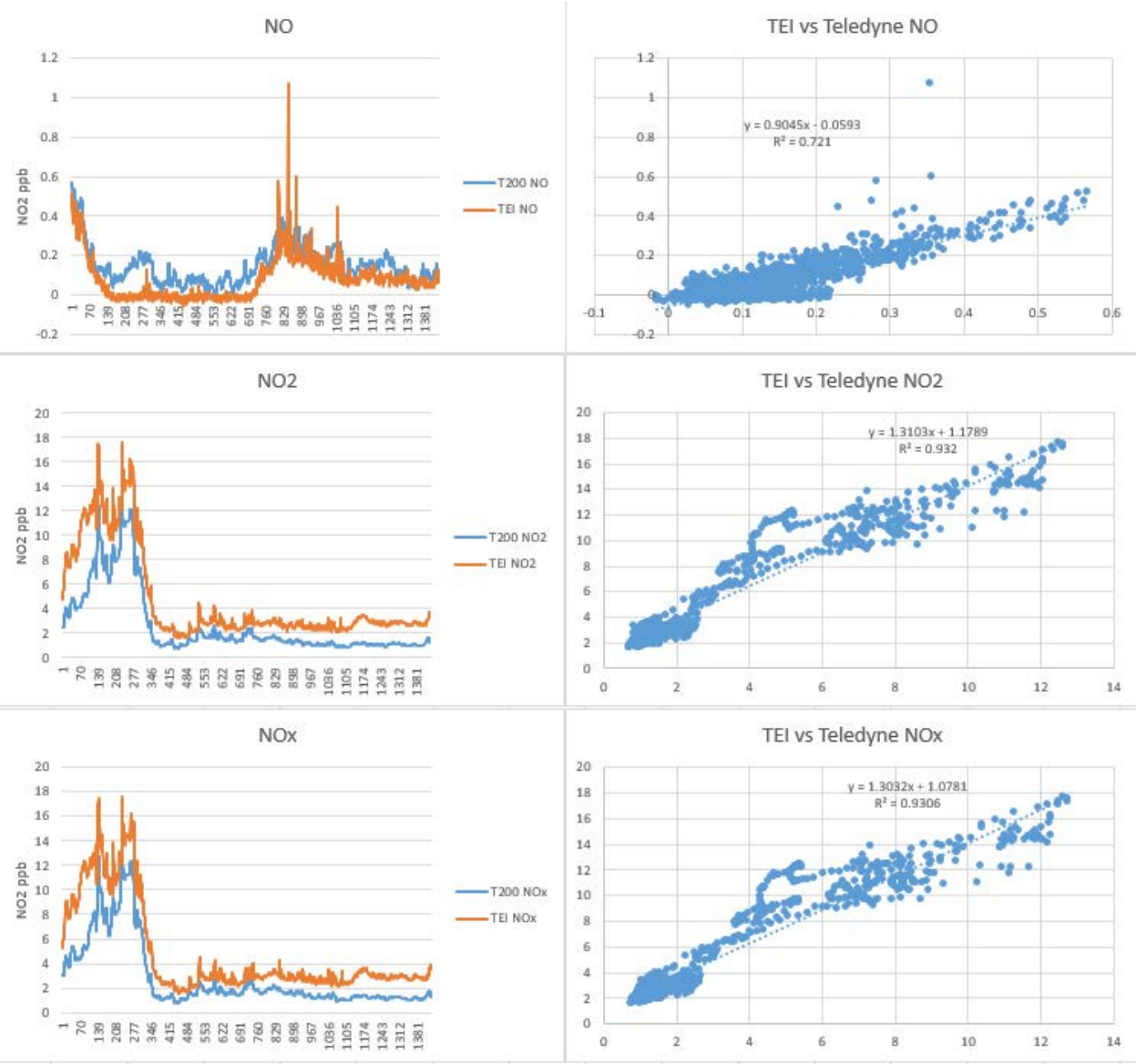

Figure SE3:
Monitoring results for nitric oxide (NO), nitrogen dioxide (NO_2), and NO_x (NO + NO_2) from the side-by-side operation of both analyzers at LUR on June 14, 2020. The graphs on the left show the time series results over the 24-hour time interval (x-axis scale is in minutes after midnight). Graphs on the right show the linear regression results with the data from the Thermo Scientific (TEI) analyzer (y-axis) plotted against the Teledyne analyzers (x-axis). The linear regression results from the comparison are added to the graphs.

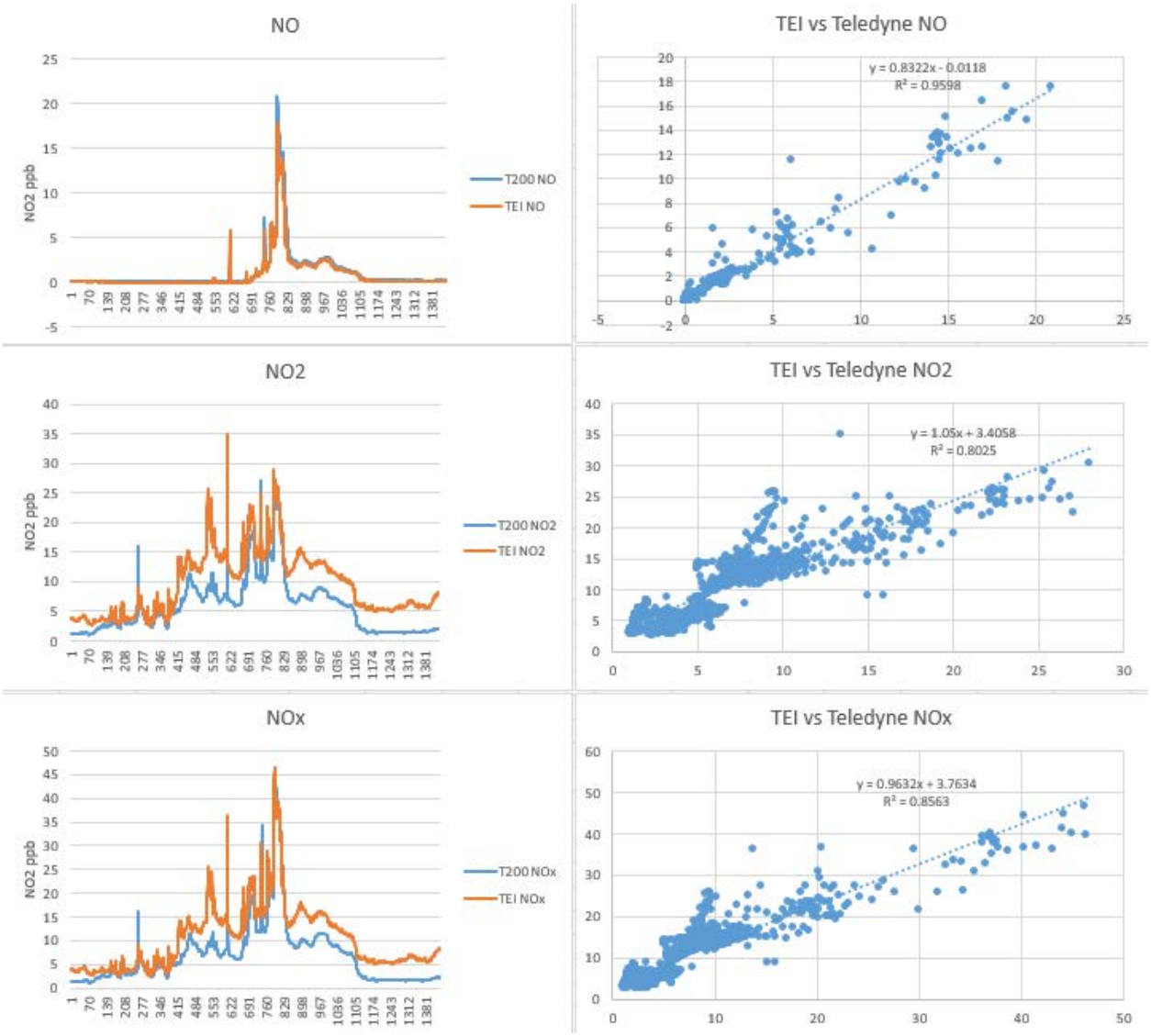

Figure SE4:
Monitoring results for nitric oxide (NO), nitrogen dioxide (NO_2), and NO_x (NO + NO_2) from the side-by-side operation of both analyzers at LUR on June 15, 2020. The graphs on the left show the time series results over the 24-hour time interval (x-axis scale is in minutes after midnight). Graphs on the right show the linear regression results with the data from the Thermo Scientific (TEI) analyzer (y-axis) plotted against the Teledyne analyzers (x-axis). The linear regression results from the comparison are added to the graphs.

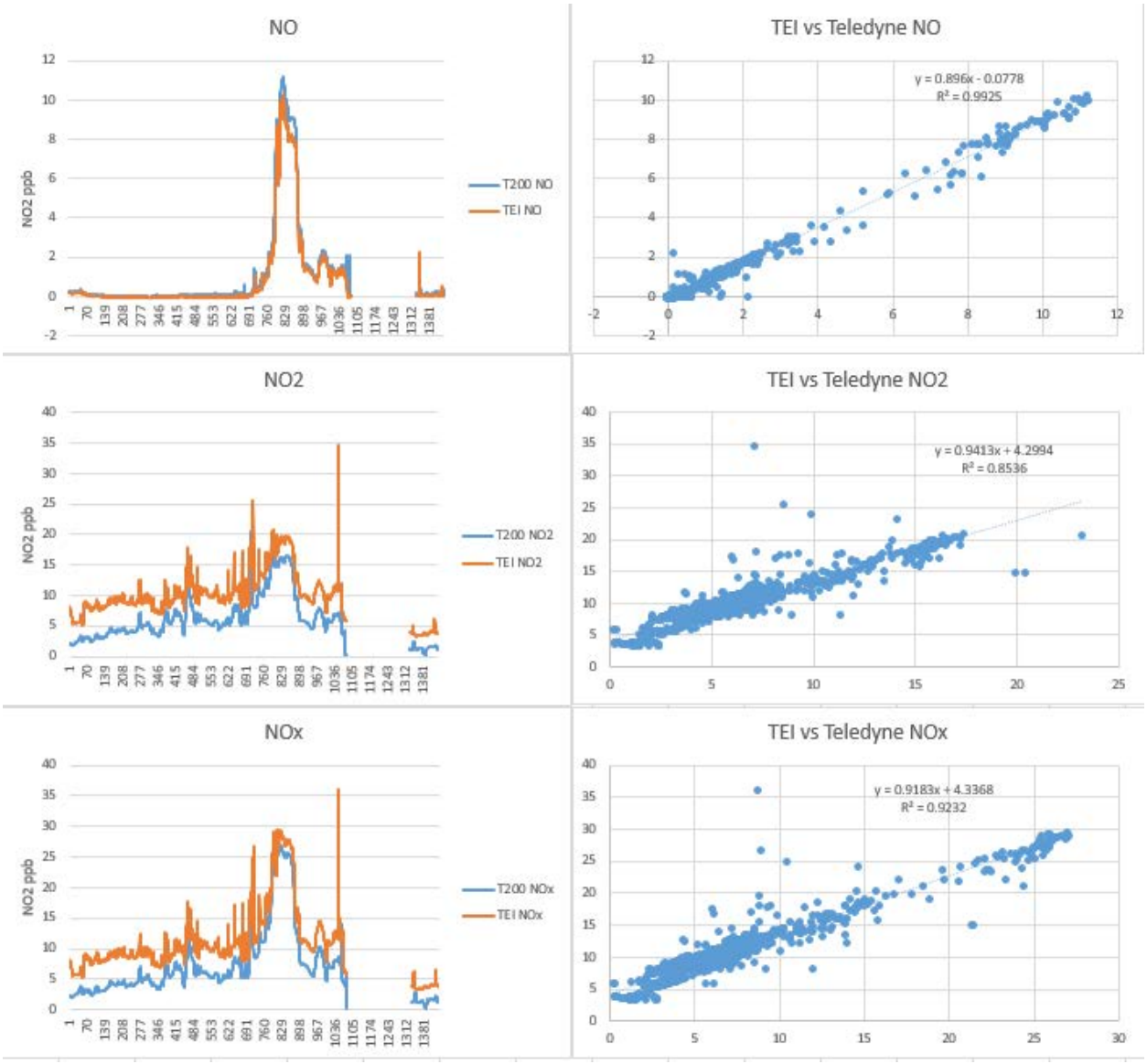

Figure SE5:
Monitoring results for nitric oxide (NO), nitrogen dioxide (NO_2), and NO_x (NO + NO_2) from the side-by-side operation of both analyzers at LUR on June 16, 2020. The graphs on the left show the time series results over the 24-hour time interval (x-axis scale is in minutes after midnight). Graphs on the right show the linear regression results with the data from the Thermo Scientific (TEI) analyzer (y-axis) plotted against the Teledyne analyzers (x-axis). The linear regression results from the comparison are added to the graphs.

Table SE1
Corrections (offsets) that were determined for the LUR NO_x monitoring with the Thermo Scientific 42iQ analyzer.

	Jan-20	Feb-20	Mar-20	Apr-20	May-20	Jun-20
2% tile BRZ	0.447	0.537	0.866	0.977	0.95	0.587
2% tile BSE				0.477	0.631	0.315
AVG 2% tile	0.447	0.537	0.866	0.727	0.7905	0.451
2% tile LUR	2.072	4.345	3.138	3.706	3.153	1.422
Correction to apply to LUR Nox	**-1.625**	**-3.808**	**-2.272**	**-2.979**	**-2.3625**	**-0.971**